

The Madrid-2019 force field for electrolytes in water using TIP4P/2005 and scaled charges: Extension to the ions F^- , Br^- , I^- , Rb^+ , and Cs^+

Cite as: J. Chem. Phys. 156, 044505 (2022); <https://doi.org/10.1063/5.0077716>

Submitted: 05 November 2021 • Accepted: 07 January 2022 • Published Online: 26 January 2022

 S. Blazquez,  M. M. Conde,  J. L. F. Abascal, et al.



View Online



Export Citation



CrossMark

The Journal
of Chemical Physics

SPECIAL TOPIC: Low-Dimensional
Materials for Quantum Information Science

Submit Today!

AIP
Publishing

The Madrid-2019 force field for electrolytes in water using TIP4P/2005 and scaled charges: Extension to the ions F^- , Br^- , I^- , Rb^+ , and Cs^+

Cite as: J. Chem. Phys. 156, 044505 (2022); doi: 10.1063/5.0077716

Submitted: 5 November 2021 • Accepted: 7 January 2022 •

Published Online: 26 January 2022







View Online



Export Citation



CrossMark

S. Blazquez,¹  M. M. Conde,²  J. L. F. Abascal,¹  and C. Vega^{1,a)} 

AFFILIATIONS

¹ Departamento Química Física I, Facultad de Ciencias Químicas, Universidad Complutense de Madrid, 28040 Madrid, Spain

² Departamento de Ingeniería Química Industrial y Medio Ambiente, Escuela Técnica Superior de Ingenieros Industriales, Universidad Politécnica de Madrid, 28006 Madrid, Spain

^{a)} Author to whom correspondence should be addressed: cvega@quim.ucm.es

ABSTRACT

In this work, an extension of the Madrid-2019 force field is presented. We have added the cations Rb^+ and Cs^+ and the anions F^- , Br^- , and I^- . These ions were the remaining alkaline and halogen ions, not previously considered in the Madrid-2019 force field. The force field, denoted as Madrid-2019-Extended, does not include polarizability and uses the TIP4P/2005 model of water and scaled charges for the ions. A charge of $\pm 0.85e$ is assigned to monovalent ions. The force field developed provides an accurate description of aqueous solution densities over a wide range of concentrations up to the solubility limit of each salt studied. Good predictions of viscosity and diffusion coefficients are obtained for concentrations below 2 m. Structural properties obtained with this force field are also in reasonable agreement with the experiment. The number of contact ion pairs has been controlled to be low so as to avoid precipitation of the system at concentrations close to the experimental solubility limit. A comprehensive comparison of the performance for aqueous solutions of alkaline halides of force fields of electrolytes using scaled and integer charges is now possible. This comparison will help in the future to learn about the benefits and limitations of the use of scaled charges to describe electrolyte solutions.

Published under an exclusive license by AIP Publishing. <https://doi.org/10.1063/5.0077716>

I. INTRODUCTION

Life started from seas, and for this reason, water is the main component of cells. However, water alone is not in oceans since they contain a certain amount of several salts (NaCl being the most abundant component). Not surprisingly, ions are also present in living organisms. Arrhenius was the first to suggest that when salts dissolve in water, individual ions are solvated by water, and they are able to conduct the electric current so that they become electrolytes.

The solution of electrolytes in water has been studied intensively over the past century, both from an experimental point of view and from a theoretical point of view. As students, we learn the thermodynamics of electrolytes and the Debye–Hückel theory describing their activities.¹ The birth of computer simulations in the 1950s brought a new route to study these types of systems. In the 1970s, the first simulations of ionic systems were carried

out.^{2–6} Aqueous solutions of electrolytes require a force field for the molecule of water and another one for the ions in water. In the 1980s, several force fields for water were proposed (TIP3P,⁷ TIP4P,⁷ and SPC/E⁸), which are widely used nowadays. In those force fields, the molecule of water is described by using a rigid non-polarizable model, typically using a Lennard-Jones (LJ) center that is located on the oxygen and charges that are located in the protons and in other places in the molecule. In the early 2000s, new models of water were proposed, including TIP4P-Ew,⁹ TIP5P,¹⁰ and TIP4P/2005.¹¹ A common feature in these three models is that they were able to reproduce the maximum in density of pure water. It has been shown that among the rigid non-polarizable models of water, TIP4P/2005 is a quite decent one.^{12,13} When describing the force field for the ions, they are often described by a LJ center and a certain charge. The obvious option is to assign a charge of $\pm Ze$ to the ions.

Computer simulations of electrolytes are not a fully mature area. In fact, it is surprising that most of the simulation studies

dealing with these substances do not consider the possibility of evaluating properties such as freezing depression, activity coefficients, and salt solubilities. However, there has been significant progress over the last ten years and we anticipate that these properties will be computed and will bring some surprises.

There are a large number of models for different alkaline and alkaline-earth salts,^{14–42} but standard force fields do not have problems, in general (when properly designed), in reproducing the experimental densities for a particular salt, for instance, NaCl. Some force fields such as that proposed by Smith and Dang²⁰ were designed for just one electrolyte (NaCl in this case). It is more difficult to find a force field that is able to simultaneously describe the properties of a large set of salts (i.e., NaCl, KCl, and MgCl₂). Among the fields of this type, the most popular is that proposed by Joung and Cheatham²⁸ for three particular water models (TIP3P,⁷ TIP4P-Ew,⁹ and SPC/E⁸). Since TIP4P/2005¹¹ is now regarded as a good potential model for water,¹² it seems reasonable to develop a force field of electrolytes based on this potential model of water. Döpke *et al.*⁴³ have recently shown that the force field proposed by Joung and Cheatham could also be used for TIP4P/2005 [by using Lorentz–Berthelot (LB) combining rules], provided that one uses the parameters designed for either SPC/E or TIP4P-Ew. We reached a similar conclusion in 2016 when considering NaCl.⁴⁴ In any case, although the results were reasonable, it seems logical to design a force field of electrolytes, specifically for the TIP4P/2005 model of water. We started down this route in 2017 for NaCl⁴⁵ and continued in 2019 presenting a force field⁴⁶ of some ions (Li⁺, Na⁺, K⁺, Cl⁻, Mg²⁺, Ca²⁺, and SO₄²⁻) using TIP4P/2005 water. The choice of the ions in our 2019 paper was not random, but we selected the most abundant ions presented in seawater (which are also the most common ions found in the cells). We have shown that, in fact, an extremely accurate description of the properties of seawater is possible by using this force field.⁴⁷ The name of the force field designed for electrolytes in TIP4P/2005 was denoted as Madrid-2019. The purpose of this work is to extend the force field to the ions considered by Joung and Cheatham but not considered when proposing the Madrid-2019 force field, namely, the anions F⁻, Br⁻, and I⁻ and the cations Rb⁺ and Cs⁺. The motivation for this is twofold: on the one hand, to extend the applicability of the Madrid-2019 force field and, on the other hand, to allow for a direct comparison between the force field proposed by Joung and Cheatham and the Madrid-2019 force field. The difference between the Joung–Cheatham and the Madrid-2019 force field is not only the choice of the water model but also a conceptual idea that makes this comparison especially useful, as we will explain later.

Besides the density, there are some other properties that are of interest when modeling electrolytes, for instance, transport properties, such as viscosities, or individual diffusion coefficients of the ions and of water. In addition, the solubility could be of interest (as the solubility of a certain force field should not necessarily correspond to the experimental value). The overwhelming majority of the force fields proposed for electrolytes until 2011 used integer values (in electron units) of the charge of the ions in solution. How is their performance when describing the properties of these solutions? Let us briefly summarize the situation:

- Regarding transport properties, it was shown by Kim *et al.*⁴⁸ that all force fields significantly underestimated the diffusion

coefficient of water at high concentrations. In other words, the force fields overestimated the impact of the salt in the reduction of the diffusion coefficient of water.

- Yue and Panagiotopoulos⁴⁹ and also ourselves⁴⁶ showed that the viscosity of the solution is dramatically overestimated at high concentrations, sometimes having a viscosity up to 2–4 times larger than in experiments. Bearing in mind the Stokes–Einstein relation,⁵⁰ this could be expected, given the impact of the salt on the diffusion coefficient of water.
- The solubility of most of the force fields using integer charges is quite low when compared to the experiment.⁵¹ In the particular case of NaCl, the majority of models give a solubility that is too low by a factor of 2–10.^{52–56} However, it is clear after the work of Yagasaki *et al.*⁴² that when properly designed, the use of integer charges still allows for a good description of the solubility. Calculating solubilities via computer simulations is difficult and only feasible in the last 10 years. For this reason, all force fields proposed before 2011 did not consider solubility as a property of interest. Therefore, although the use of integer charges should not necessarily provoke a low solubility, it turns out that this was the case for practically all force fields previously designed using integer charges.
- Related to the previous point is the finding that for a number of force fields of electrolytes, the number of contact ion pairs (CIPs) (i.e., a cation in contact with an anion in solution^{57–60}) was quite high and aggregation of ions (which can be regarded as the initial step of precipitation) was observed in many simulations even at concentrations well below the experimental solubility⁶¹ (reflecting that the solubility of the force field was well below the experimental one). Actually, ion clustering has been reported for different salts below its experimental solubility limit. This fact can be seen in monovalent salts as NaCl,^{26,62–64} KCl,⁶⁵ and divalent salts CaCl₂⁶⁶ or even sulfates as Na₂SO₄⁶⁷ and Li₂SO₄.⁶⁸

How to go to the next generation of force fields for electrolytes? *Ab initio* calculations can be useful, as shown by Ding *et al.*,⁶⁹ but these types of calculations are quite expensive from a computational point of view. Introducing polarizability is another possibility (see the work of Kiss and Baranyai^{38,70}), and certainly, further research will continue to appear in this area. Note that including polarization does not guarantee good solubilities, as shown for the Baranyai force field.⁵⁶ However, it is possible to modify the parameters to improve their predictions.³⁹ First-principles calculations and polarizable models will continue to be developed in the future. However, there is a simple and cost-effective approach that could improve the performance without extra computational cost. The recipe is simple, and it amounts to using scaled charges for the ions (i.e., force fields in which the charge of the ions is λe , where λ is a number smaller than one). The use of scaled charges is common in simulations of ionic liquids,^{71–75} so exploring this route for electrolytes seems to be of interest.

Let us briefly describe the “history” of scaled charge models. This was first suggested by Leontyev and Stuchebrukhov,^{76–81} by

realizing that the dielectric constant at high frequencies of non-polarizable models is 1, whereas for water, its value is 1.78. With that in mind, Leontyev and Stuchebrukhov suggested using a scaled charge of $q_{\text{scaled}}(e) = 1/\sqrt{\epsilon_{\infty}}$ for the ions. This leads to a charge of $0.75 Ze$ for the ions in water. This suggestion was further expanded by Jungwirth and co-workers,^{66,68,82-84} and they have developed a potential model for several ions using this value for the charge of the ions. Kann and Skinner followed a somewhat different approach.⁸⁵ If you want to recover the Debye–Hückel law, you should have a force field, accurately describing the density of water, where the strength of the Coulombic energy between ions at infinite dilution and infinitely large distances should be identical in your model and in the experiment. Many force fields of water do not reproduce the experimental value of the dielectric constant of pure water, and scaled charges should be used to recover the Debye–Hückel law. In the particular case of TIP4P/2005, this results in a value of $0.85 Ze$.⁸⁵ One of us has also pointed out that different charges may be needed to describe the potential energy surface and the dipole moment surface.⁸⁶ Note that for water models without charges, such as mW,⁸⁷ it is possible to design a force field for electrolytes without charges, as is the route followed by DeMille and Molinero, and still obtain good results.⁸⁸ Fuentes-Azcatl and Barbosa⁸⁹ also used scaled charges. Li and Wang⁹⁰ and Bruce and van der Vegt⁹¹ also explored the use of scaled charges. The effect of charge transfer was also studied by Rick and co-workers,⁹²⁻⁹⁵ suggesting that part of the charge of the ions is transferred to the adjoining water molecules, as also later shown by Yao *et al.*⁹⁶ This charge transfer implies that the charge of the ions is not unity and has also been confirmed by quantum calculations.⁵⁹ The community using scaled charges is growing, and Jungwirth and co-workers summarized the situation in a couple of review papers.^{97,98}

In our previous studies in 2017⁴⁵ and in 2019,⁴⁶ we have shown that the use of scaled charges improves the description of the solubility (at least for NaCl), and the same is true for the viscosity and the diffusion coefficient of water. Yue and Panagiotopoulos presented further evidence of that.⁴⁹ In fact, we have shown recently that more complex phenomena such as the salting out effect of methane can be quantitatively described with the use of scaled charges.⁹⁹ Thus, scaled charges seem to improve the description of aqueous solutions of electrolytes. Scaled charges cannot describe everything. In fact, they cannot describe the melt, the solid, the vapor–liquid equilibrium of the molten salts, or the kinetics of precipitation.^{51,100} Scaled charges are useful only when describing the properties of aqueous solutions of electrolytes but not in problems where the system does not contain water (or has a very small amount).

To sum up in this paper, we extend the Madrid-2019⁴⁶ force field to other monovalent cations and anions belonging to the alkaline group and to halogens. By doing that, we now have a set of parameters for the same set of ions selected by Joung and Cheatham²⁸ and ready for their use with the TIP4P/2005¹¹ model of water that was not considered in the original parameterization of Joung and Cheatham. A consequence is that now, a face to face comparison of a good force field designed using integer charges and a force field designed using scaled charges is possible. We hope that this comparison will shed light on the possible advantages and disadvantages of the use of scaled charges for modeling electrolyte solutions.

II. EXTENDING THE MADRID-2019 FORCE FIELD TO OTHER ELECTROLYTES

In this work, an extension (to other ions) of the recently developed Madrid-2019⁴⁶ force field of scaled charges has been carried out. The Madrid-2019⁴⁶ force field was initially proposed to describe the most common salts present in seawater. In this work, we extend the model to the rest of the halogens that remained to be studied (F^- , Br^- , and I^-) and to the rest of the cations of the alkaline group (Rb^+ and Cs^+). When designing force fields, certain properties are used as the target, and the values of the parameters of the potential are obtained so that these properties are reproduced.

Now, we describe in detail the philosophy of the Madrid-2019 force field and the approach we used to obtain the parameters of the potential. Obtaining parameters of a force field is a difficult job. It requires patience, a good design, and some trial and error. In the future, machine learning techniques could certainly help in obtaining the best set of parameters for a certain potential model. It should be recognized from the very beginning that the only way to reproduce experimental results for all properties would be to solve the Schrödinger equation exactly and to include nuclear quantum effects. If this is not done, your approach will not be able to reproduce “everything” and certain properties will be reproduced, but other properties will not be. These are the main characteristics of the Madrid-2019 force field and the description of how the parameters were obtained:

- Water is described by using the TIP4P/2005 model. Ions are described by a Lennard-Jones (LJ) center and a certain charge. In the case of the Madrid-2019 force field, the charge (in electron units) is scaled and its value is 0.85 for monovalent ions and 1.70 for divalent ions. The force field requires one to know the LJ parameters (σ and ϵ) of the interaction of a certain ion with the rest of species of the system.
- The Lennard-Jones interaction between an ion and water is described by the ion–oxygen interaction (i.e., there is no ion–hydrogen interaction). The reason for that is that in the TIP4P/2005 model of water, there is no LJ center on the hydrogen atoms of the molecule of water.
- Lorentz–Berthelot (LB) rules are, in general, not used. Thus, the parameters of the LJ ion–oxygen interaction between a cation and an anion are not obtained via the LB combination rule. However, the interaction between two different types of cations and/or two different types of anions (required to study systems having simultaneously several salts as in the case of seawater) is usually given by LB combining rules.
- The force field is transferable. The parameters of the interaction of an ion with other species (water, other ions, etc.) are always the same regardless of the chemical composition of the system.
- In this work, the parameters for the interaction between Cl^- , Li^+ , Na^+ , K^+ , Mg^{2+} , and Ca^{2+} ions with water and the crossed interactions between these ions are taken from our previous work in which the Madrid-2019⁴⁶ force field was introduced. This is an advantage as it reduces the number of parameters to be determined.
- The density of solutions is always considered as a target property. The density of ionic solutions is known with high

accuracy from experiments, and we always use it as the target property (at room temperature and pressure).

- The LJ parameters of the ion–water interaction were determined by using the experimental densities for low concentrations (typically up to 1–2 molal, i.e., less than 1–2 mols of salt per kilogram of water). The reason for that is that at low concentrations, the properties of the solution are mainly given by the ion–water interaction and the impact of ion–ion interaction at low concentrations is quite small. As an example to determine the properties of bromide salts, we shall consider the experimental densities of LiBr, NaBr, KBr, MgBr₂, and CaBr₂ and will determine the parameters of the Br[−]–water interaction using the experimental densities (up to 1–2 m) as the target. Note that for these salts, the cation–water interaction is already available for the Madrid-2019 force field, so we only need to determine the LJ parameters of the Br[−]–water interaction.
- Obtaining the Br[−]–Br[−] and Br[−]–cation interactions (we shall use Br[−] as an example to illustrate how the force field was obtained) is a somewhat more involved process. Again, we shall consider the experimental properties of LiBr, NaBr, KBr, MgBr₂, and CaBr₂ and used the Madrid-2019 force field for the cation–cation interaction. Thus, one needs to determine the Br[−]–cation interactions and the Br[−]–Br[−] interaction. This was done using three target properties. The density of the melt should be reproduced (i.e., we used as the target a density 20%–25% lower than the experimental one). The experimental density of the ionic solutions at high concentrations (close to the experimental solubility limit) should be reproduced. The third constraint is the number of contact ion pairs (CIPs). In the study of aqueous electrolyte solutions, it is important to evaluate the number of CIPs. High values of CIPs indicate (indirectly) cluster formation and/or precipitation of the salt. Benavides *et al.*¹⁰¹ suggested in a previous work that for 1:1 electrolytes with the solubility lower than 11 m, the number of CIPs must be below 0.5 to be sure that precipitation and/or aggregation of ions has not occurred. This rule will be important in the majority of the salts of this work. (We will discuss later the number of CIPs for exceptional cases, such as salts with extremely high solubilities.) Thus, obtaining Br[−]–Br[−] and Br[−]–cation interaction is the most difficult step. The reader may wonder why we did not try to reproduce the experimental densities of the melt with scaled charges. We explored this approach but found that often the salt in solution had a large number of CIPs and, in some cases, precipitated. For instance, for NaBr, we were able to find a set of parameters describing the melt quite well (using scaled charges), but with these parameters, the number of CIPs in the aqueous solution was large (3.4 at 8 m) and the salt precipitated spontaneously. Thus, it seems that to obtain a correct balance between ion–water and ion–ion interactions when using scaled charges, the target density of the melt should be somewhat smaller (20%–25%) than the experimental value.

The last step described above, i.e., obtaining, for instance, Br[−]–Br[−] and Br[−]–cation interactions, requires some further clarifications. The density of the melt is used as a target property. We

prefer the melt with respect to the ionic solid as when using empirical force fields, the mechanical stability of the experimental solid structure is not guaranteed. Besides this, in the melt, one would sample anion–anion, cation–cation, and anion–cation interactions. However, the target density was not the experimental density of the melt, but a density typically around 20%–25%, lower than the experimental one. The reason for that is that we recognize from the very beginning that scaled charges are not adequate to reproduce the properties of pure ionic systems, as was pointed out by Panagiotopoulos and co-workers.^{51,100} We observed that when using scaled charges for the melt, one obtains a density 20%–25% lower than the experimental value and a reasonably low number of CIPs, avoiding precipitation of the system. However, when replacing the charge with integer values (while keeping the LJ parameters), the experimental density of the melt is reproduced. Our approach will allow one in the future to design and develop a force field in which the charge of the ions is sensitive to the local environment within the spirit of polarizable models.

In addition, it is interesting to point out that ideally, the solubility of the salt should be considered as a target property. If the solubility is low, then the ions will tend to cluster in solution (or even precipitate spontaneously) and the results of the force field would be unreliable. The calculation of the solubility of a salt is difficult from a computational point of view, and evaluating it for several trial values of the potential parameters would be beyond current computational limits. However, there is a rather simple approach, at least to avoid low values of the solubility.

We have shown in the past for salts with solubilities smaller than 11 m that the number of CIPs at the solubility limit of the model is less than 0.5.¹⁰¹ Thus, having a number of CIPs larger than 0.5 is a warning, which indicates that we are not that far from the solubility of the model and the risk of spontaneous precipitation exists (although since nucleation is an activated process, precipitation may occur at concentrations several times higher than the solubility limit, as it happens for the JC-SPC/E model of NaCl^{102,103}). Therefore, we will always force the force field to have a number of CIPs less than 0.5 at the experimental value of the solubility (whenever below 11 m). For salts with higher solubilities, we will discuss later the number of CIPs.

In summary, the main goal of the Madrid-2019 force field is to reproduce thermodynamic and transport properties of ionic solutions, sacrificing somehow the properties of the melt and/or the solid. The main property of the solution that cannot be reproduced by the introduction of scaled charges is the free energy of hydration, which will be low compared to experiments (although it can be corrected in a theoretical way⁹⁹). Nikitin and Del Frate¹⁰⁴ pointed out that the calculation of the total free energy of hydration, ΔG , is better (when including a theoretical correction) by using

TABLE I. Force field parameters for water TIP4P/2005 parameters from Ref. 11.

Molecule	Charge (e)	σ_{ii} (Å)	ϵ_{ii} (kJ/mol)
TIP4P/2005			
O	0	3.1589	0.7749
H	0.5564		
M	−1.1128		

TABLE II. Lennard-Jones parameters σ_{ij} (in Å) for the Li^+ , Na^+ , K^+ , Rb^+ , Cs^+ , Mg^{2+} , Ca^{2+} , F^- , Cl^- , Br^- , I^- , and SO_4^{2-} ions. O_w and O_s represent the water and sulfate oxygens.

	F^-	Cl^-	Br^-	I^-	Li^+	Na^+	K^+	Rb^+	Cs^+	Mg^{2+}	Ca^{2+}	O_w	S	O_s
F^-	3.789 82	LB	LB	LB	2.845 40	LB	3.462 50	3.572 50	3.945 50	LB	LB	3.774 50	LB	LB
Cl^-		Madrid-2019	LB	LB	Madrid-2019	Madrid-2019	Madrid-2019	3.996 42	4.318 54	Madrid-2019	Madrid-2019	Madrid-2019	Madrid-2019	Madrid-2019
Br^-			4.825 25	LB	2.614 50	3.385 00	3.798 79	3.917 25	4.334 08	2.655 19	3.670 52	4.198 50	LB	LB
I^-				5.049 75	3.204 70	3.646 58	4.005 50	4.102 88	4.437 90	2.827 07	3.941 81	4.349 50	LB	LB
Li^+					Madrid-2019	Madrid-2019	Madrid-2019	LB	LB	Madrid-2019	Madrid-2019	Madrid-2019	Madrid-2019	Madrid-2019
Na^+					Madrid-2019	Madrid-2019	Madrid-2019	LB	LB	Madrid-2019	Madrid-2019	Madrid-2019	Madrid-2019	Madrid-2019
K^+								2.994 98	LB	LB	LB	3.543 50	LB	3.400 00
Rb^+									3.521 013	LB	LB	3.662 90	LB	LB
Cs^+										Madrid-2019	Madrid-2019	Madrid-2019	Madrid-2019	Madrid-2019
Mg^{2+}											Madrid-2019	Madrid-2019	Madrid-2019	Madrid-2019
Ca^{2+}											Madrid-2019	Madrid-2019	Madrid-2019	Madrid-2019
O_w												Madrid-2019	Madrid-2019	Madrid-2019
S													Madrid-2019	Madrid-2019
O_s														Madrid-2019

TABLE III. Lennard-Jones parameters ϵ_{ij} (in kJ/mol) for the Li^+ , Na^+ , K^+ , Rb^+ , Cs^+ , Mg^{2+} , Ca^{2+} , F^- , Cl^- , Br^- , I^- , and SO_4^{2-} ions. O_w and O_s represent the water and sulfate oxygens.

	F^-	Cl^-	Br^-	I^-	Li^+	Na^+	K^+	Rb^+	Cs^+	Mg^{2+}	Ca^{2+}	O_w	S	O_s
F^-	0.030 963 7	LB	LB	LB	0.110 265 5	LB	0.223 167	0.216 120 2	0.097 105	LB	LB	0.1000	LB	LB
Cl^-		Madrid-2019	LB	LB	Madrid-2019	Madrid-2019	Madrid-2019	0.340 641	0.161 555 8	Madrid-2019	Madrid-2019	Madrid-2019	Madrid-2019	Madrid-2019
Br^-			0.112 795	LB	0.199 378	0.356 77	0.425 940	0.458 323	0.195 632	0.641 807	0.239 185	0.1000	LB	LB
I^-				0.179 01	0.273 498	0.513 387	0.536 590	0.519 646	0.246 452	0.808 534	0.301 320	0.1000	LB	LB
Li^+					Madrid-2019	Madrid-2019	Madrid-2019	LB	LB	Madrid-2019	Madrid-2019	Madrid-2019	Madrid-2019	Madrid-2019
Na^+					Madrid-2019	Madrid-2019	Madrid-2019	LB	LB	Madrid-2019	Madrid-2019	Madrid-2019	Madrid-2019	Madrid-2019
K^+								1.862 314	LB	LB	LB	0.1000	LB	1.250 800
Rb^+									0.375 959 6	LB	LB	0.1000	LB	LB
Cs^+										Madrid-2019	Madrid-2019	Madrid-2019	Madrid-2019	Madrid-2019
Mg^{2+}											Madrid-2019	Madrid-2019	Madrid-2019	Madrid-2019
Ca^{2+}											Madrid-2019	Madrid-2019	Madrid-2019	Madrid-2019
O_w												Madrid-2019	Madrid-2019	Madrid-2019
S													Madrid-2019	Madrid-2019
O_s														Madrid-2019

scaled charges. They considered that the total hydration energy can be divided into two terms: one is calculated in simulations ΔG_{MD} and the other one is a theoretical correction denoted as the electronic polarization (ΔG_{el}). That resembles the situation for water of models such as SPC/E,⁸ TIP4P-Ew,⁹ or TIP4P/2005¹¹ that sacrifice the enthalpy of vaporization of water as a target property (in contrast with TIP3P,⁷ TIP4P,⁷ and TIP5P¹⁰) to obtain an overall better description of its properties. Note, though, that activity coefficients, osmotic pressures, and a number of properties of solution could still be reproduced even though the absolute value of the hydration free energy is not reproduced. This is so because what really matters is the variation of the Gibbs free energy of the system with the addition of salt, rather than the absolute values of the Gibbs free energies. Transfer of a salt either from vacuum or from a hydrophobic solvent to water will not be described properly by using scaled charges, but this is not a big problem as ions are usually not found either in vacuum or in hydrophobic solvents due to the low concentration of ions often found in these two media. Note that Vazdar *et al.*¹⁰⁵ showed in 2012 that using scaled charges (i.e., an electronic continuum correction) allows us to describe reasonably well the hydrophobic oil/water interface. In general, they proposed that interfaces with no electronic discontinuity can be reasonably described by using scaled charges.

We shall now present the parameters of the Madrid-2019 force field extended to the new ions (F^- , Br^- , I^- , Rb^+ , and Cs^+). We shall denote this as Madrid-2019-Extended. The interaction between atoms can be described by two different contributions: an electrostatic (Coulombic) contribution and a van der Waals interaction, represented by the LJ potential,

$$u(r_{ij}) = \frac{1}{4\pi\epsilon_0} \frac{q_i q_j}{r_{ij}} + 4\epsilon_{ij} \left[\left(\frac{\sigma_{ij}}{r_{ij}} \right)^{12} - \left(\frac{\sigma_{ij}}{r_{ij}} \right)^6 \right], \quad (1)$$

where q_i is the ionic charge, ϵ_0 is the vacuum permittivity, ϵ_{ij} is the well depth energy of the LJ potential, and σ_{ij} is the LJ diameter.

Let us now describe the TIP4P/2005 model of water developed by Abascal and Vega.¹¹ In this model, based on the TIP4P water proposed by Jorgensen *et al.*,⁷ water molecules have four atoms: two hydrogens with charge q_H ; one oxygen, which is a LJ site but has no charge; and one point M, near the oxygen atom on the symmetric axis, without mass but with charge q_M . The geometry of water molecules for the TIP4P/2005 model can be described by the following parameters: oxygen–hydrogen distance, $d_{OH} = 0.9572$ Å, oxygen–M distance, $d_{OM} = 0.1546$ Å, and angle H–O–H = 104.52° . TIP4P/2005 parameters are shown in Table I.

We proceed now to present the Madrid-2019-Extended model parameters, which are shown in Tables II and III. We only show the parameters obtained in this work, (when for a certain interaction one reads LB, it means that the interaction has been obtained from the application of the LB combining rule). The salts developed in the Madrid-2019 original model⁴⁶ are denoted as Madrid-2019.

In Table IV, we show experimental melting temperatures and solubility limits for the salts considered in this work. As can be seen, with the exception of LiF and NaF, which have low solubilities, the rest of the salts have medium and high solubilities. In the case of fluorides (KF, RbF, and CsF), the solubility is extremely high, even reaching a solubility of 37 m for CsF. The solubility of LiBr, used in energy conversion processes, is also high (see Table IV).

TABLE IV. Experimental melting temperature for anhydrous salt¹⁰⁶ and salt solubility in water¹⁰⁶ at 25 °C reported in molality units for the salts studied in this work.

Salt	Melting temperature (K)	Solubility at 25 °C (mol/kg)
LiF	1121.35	0.052
LiBr	825.15	20.84
LiI	742.15	12.33
NaF	1269.15	0.99
NaBr	1020.15	9.20
NaI	933.15	12.4
KF	1131.15	17.50
KBr	1007.15	5.77
KI	954.15	8.92
RbF	1106.15	28.8
RbCl	988.15	7.77
RbBr	955.15	7.01
RbI	915.15	7.76
Rb ₂ SO ₄	1323.15	1.90
CsF	976.15	37.7
CsCl	918.15	11.3
CsBr	909.15	5.77
CsI	894.15	3.26
Cs ₂ SO ₄	1278.15	5.03
MgBr ₂	984.15	5.6
MgI ₂	907.15	5.2
CaBr ₂	1015.15	7.65
CaI ₂	1056.15	7.3

III. SIMULATION DETAILS

We have studied different properties to test our extended model. Molecular Dynamics (MD) simulations have been carried out using the GROMACS package^{107,108} in the NpT and NVT ensembles. In all the runs, the leap-frog integrator algorithm¹⁰⁹ with a time step of 2 fs was used. We also applied periodic boundary conditions in all directions in all cases. The temperature was kept constant using the Nosé–Hoover thermostat^{110,111} with a coupling constant of 2 ps. The Parrinello–Rahman barostat¹¹² with a time constant of 2 ps was implemented to keep constant pressure in NpT simulations (1 bar for all simulations). For electrostatics and van der Waals interactions, the cut-off radii were fixed at 1.0 nm and long-range corrections to the Lennard-Jones part of the potential in the energy and pressure were applied. The smooth PME method¹¹³ to account for the long-range electrostatic forces was used. Water geometry was maintained using the LINCS algorithm.^{114,115}

Most of the results of this work (unless otherwise stated) for aqueous solutions were obtained from NpT simulations using 555 molecules of water and from runs lasting 50 ns. Densities, water diffusion coefficients, and radial distribution functions (RDFs) were obtained from these runs. The choice of the number of water molecules is useful because for 1:1 electrolytes, adding ten cations and ten anions would yield a solution being ~1 m (i.e., 1 mol of salt per kilogram of water). A property of interest is the number of CIPs, which represents the number of anions that is in close contact with a cation (i.e., without a molecule of water between the two

ions). The number of CIPs of the cation is evaluated easily from the cation–anion pair correlation function as

$$n^{CIP} = 4\pi\rho_- \int_0^{r_{\min}} g_{\pm}(r) r^2 dr, \quad (2)$$

where g_{\pm} is the cation–anion radial distribution function (RDF); ρ_- is the number density of anions (the number of anions per unit of volume); and r_{\min} (the integral upper limit) is the position of the first minimum in the RDF, which must be located at a similar distance to that of the cation– O_w RDF. One can simultaneously plot the RDFs cation–anion and cation– O_w to determine if we are really evaluating the CIP or a contact solvent separated ion pair (CSSIP, which corresponds to a cation in contact with an anion but with a molecule of water between them). The hydration numbers (i.e., the number of water molecules around each ion) can also be calculated by a similar equation to Eq. (2) but replacing ρ_- with ρ_w (i.e., the number density of water obtained by dividing the number of molecules of water between the volume of the simulation box) and $g_{\pm}(r)$ with $g_{ion-O_w}(r)$ instead.

The Einstein relation was used to calculate diffusion coefficients

$$D = \lim_{t \rightarrow \infty} \frac{1}{6t} \langle [\bar{r}_i(t) - \bar{r}_i(t_0)]^2 \rangle, \quad (3)$$

where $\bar{r}_i(t)$ and $\bar{r}_i(t_0)$ are the position of the i th particle at time t and a certain origin of time t_0 and the $\langle [\bar{r}_i(t) - \bar{r}_i(t_0)]^2 \rangle$ term is the mean square displacement (MSD). From the plot of the MSD vs time, a slope can be obtained, which is six times the diffusion coefficient.

A somewhat larger system having 4440 molecules of water (i.e., eight times 555) was considered to evaluate viscosities and the possible existence of precipitation. The methodology used to compute the viscosity is similar to that described in previous works.¹¹⁶ We perform a previous NpT simulation to accurately calculate the volume of the system. After that, a NVT simulation of 50 ns was performed. Throughout the run, the pressure tensor $P_{\alpha\beta}$ was calculated and saved on disk every 2 fs. The off-diagonal elements of the pressure tensor are P_{xy} , P_{xz} , and P_{yz} , which are equivalent. In addition, due to the rotational invariance of the molecules, the terms $(P_{xx} - P_{yy})/2$ and $(P_{yy} - P_{zz})/2$ are also equivalent.^{117,118} Thus, we have averaged the five pressure components in order to obtain accurate results. Finally, the Green–Kubo formula for the viscosity was used,

$$\eta = \frac{V}{kT} \int_0^{\infty} \langle P_{\alpha\beta}(t_0) P_{\alpha\beta}(t_0 + t) \rangle_{t_0} dt. \quad (4)$$

The upper limit of the integral is usually between 10 and 20 ps.

Aggregation and precipitation will spoil the results of any simulation, giving unphysical results. We have not determined the solubility of the salts considered in the force field of this work. However, we have performed a simple test. We have performed a long run of 50 ns at the experimental value of the solubility limit of each salt, using a large system having 4440 molecules of water (since nucleation time decreases with system size, we used a large system to be on the safe side) and with the number of ions required to mimic the experimental value of the solubility and checked for the absence of precipitation. The absence of precipitation was checked in several ways, such as visually analyzing the trajectories, analyzing the final configuration of the run, from a dynamic increase of the number of CIPs, and from the possible existence of a drift in the thermodynamic properties. For all the salts considered in this work, we found

no evidence of precipitation at the experimental value of the solubility limit. Of course, this does not guarantee that the force field in this work has the correct solubility. It only guarantees that the salt is either stable or metastable at the experimental value of the solubility limit and that the presented results are not an artifact due to the existence of spontaneous precipitation.

Molten densities were obtained for systems containing 1000 ions. Simulations typically lasted 50 ns in NpT simulation at 1 bar and at the melting temperature of the salt. We usually performed simulations with integer charges first (with densities close to the experimental values) and then used the final configuration as the initial one for NpT runs using scaled charges to observe the decrease in density provoked by the use of scaled charges. The average densities were obtained from the last 20 ns of the run, after the system was fully relaxed.

IV. RESULTS

A. Finding parameters for Rb^+ and Cs^+ : Chloride salts

We shall start by presenting results for chloride salts as they were obtained to determine parameters for Rb^+ and Cs^+ (i.e., $Rb^+ - Rb^+$, $Cs^+ - Cs^+$, $Rb^+ - Cl^-$, $Cs^+ - Cl^-$, and, more importantly, $Rb^+ - water$ and $Cs^+ - water$ interactions). When developing the Madrid-2019-Extended force field, we typically used the following strategy. We considered a salt (or several) with formula XY , either X (or Y) being an ion not present in the Madrid-2019 force field and either Y (or X) being an ion for which parameters are available in the Madrid-2019 force field. For instance, to determine parameters for Rb^+ , we shall use as target properties those of the $RbCl$ salt. We used this salt to obtain the $Rb^+ - water$ interaction. As mentioned before, $Rb^+ - Cl^-$ and $Rb^+ - Rb^+$ interactions were determined by fitting the properties of the melt and keeping the number of CIPs within reasonable limits. We follow a similar procedure to determine the parameters of Cs^+ .

In Fig. 1, the densities from experiments are compared to the simulation results obtained from the Madrid-2019-Extended force field for concentrations up to the experimental value of the solubility limit. As can be seen, the agreement is quite good. Only at high concentrations are the experimental values slightly underestimated. The statistical error in the densities calculated in this work is always less than 0.25%.

Next, we computed the viscosity. The results are shown in Fig. 2. The statistical error in the viscosities calculated in this work is always less than 5%–10% (being lower at low concentrations of salt). Experimentally, the viscosity of a $RbCl$ solution does not change much with concentration, decreasing slightly at low concentrations, having a weak minimum, and then increasing slightly. Simulations are not able to capture this subtle behavior. In addition, it is clear that the model overestimates the viscosity with respect to experimental values. However, the model is able to predict that the change in the viscosity of a $RbCl$ solution with respect to water is much smaller than that of a $NaCl$ or KF solution at similar concentrations, as will be discussed later in this paper. Further work is needed to understand the origin of this discrepancy. We checked for the possible existence of spontaneous precipitation in simulations. However, we found no evidence of precipitation at the highest concentration considered so that this is not at the origin of the discrepancy.

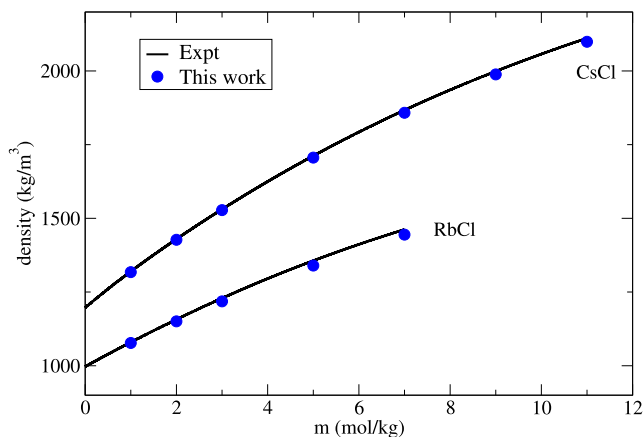


FIG. 1. Density as a function of molality at $T = 298.15$ K and 1 bar for chloride salts of aqueous solutions, RbCl and CsCl. Blue circles: this work. Black solid lines: fit of experimental data taken from Ref. 119. CsCl values were shifted up 200 density units for better legibility.

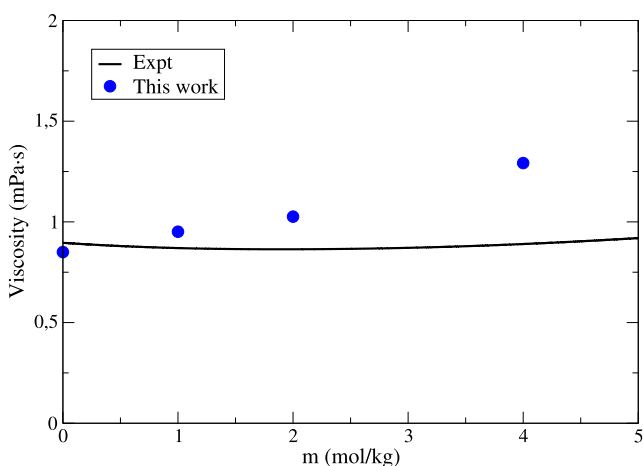


FIG. 2. Shear viscosity curves as a function of concentration for aqueous RbCl solutions at 298.15 K and 1 bar. The blue circles represent the results from this work. The continuous lines represent the fit of experimental data taken from Ref. 120.

Structural properties are presented in Table V. Before describing the structural properties of the following chloride salts, it is important to point out that the experimental data with which we compare were measured, in general, at low concentrations, and for this reason, they only depend on the ion being studied and not on the particular salt. Regarding, specifically, chloride salts, it can be seen that the hydration number of the cation at high concentration is around 6. The number of CIPs is below 0.5 for both salts. For RbCl, the number of CIPs is 0.23 at 7 m, and for CsCl, it is 0.48 at 11 m. Thus, these cations have around 6.3 (Rb^+) or 6.6 (Cs^+) particles around them. At high concentrations, ions can replace water molecules (although due to the different sizes, the replacement is not one to one). The distance at which first the peak appears for the cation–oxygen radial distribution function is slightly smaller than that found in experiments. However, densities are predicted well, as can be seen in Fig. 1.

B. Fluoride salts

The densities of different fluoride salts have been calculated with the Madrid-2019-Extended force field. A comparison with experimental results is shown in Fig. 3. Since the solubility of NaF is small, the results for this salt are presented separately in Fig. 3(a). (LiF was not considered as its solubility is extremely small, i.e., 0.052 m). As can be seen, the agreement with the experiment for NaF is quite good. The results for KF, RbF, and CsF are presented in Fig. 3(b). The solubilities of KF, RbF, and CsF are extremely high and increase with the size of the cation. Good agreement with the experiment is also found for these salts. For KF, RbF, and CsF, we did not find experimental results at high concentrations (even though we have evaluated the densities of these salts in the whole range of concentrations up to their solubility limit; these results are given in the supplementary material of this work). Given the accuracy of simulations at low–moderate concentrations, one could expect that simulation results at high concentrations should be reasonable.

Let us now present some results for the viscosities. Since the evaluation of the viscosity is rather expensive in this work, we shall evaluate the viscosity only for some selected salts. In Fig. 4, the results for the viscosity of the KF are presented. It can be observed that the Madrid-2019-Extended force field of this work predicts quite well the viscosities for concentrations of up to 2 m and reasonably well for the most concentrated 5 m solution. The model somewhat overestimates the experimental value. This behavior is

TABLE V. Structural properties for chloride electrolyte solutions at 298.15 K and 1 bar: number of contact ion pairs (CIPs), hydration number of cations (HN_c) and anions (HN_a), and position of the first maximum of the cation–water (d_{c-O_w}) and anion–water (d_{a-O_w}) interaction in the radial distribution function. Experimental data taken from the work of Marcus are given in parentheses.¹²¹ Properties were calculated at low concentrations and close to the solubility limit of each salt.

Salt	m (mol/kg)	CIP	HN_c	HN_a	d_{c-O_w} (Å)	d_{a-O_w} (Å)
RbCl	1	0.05	6.3(5–8)	5.8(5.3–7.2)	2.75(2.79–2.90)	3.04(3.08–3.34)
	7	0.23	6.0	5.6	2.75	3.04
CsCl	1	0.07	6.8(8–9)	5.9(5.3–7.2)	2.87(2.95–3.20)	3.04(3.08–3.34)
	11	0.48	6.0	5.5	2.85	3.04

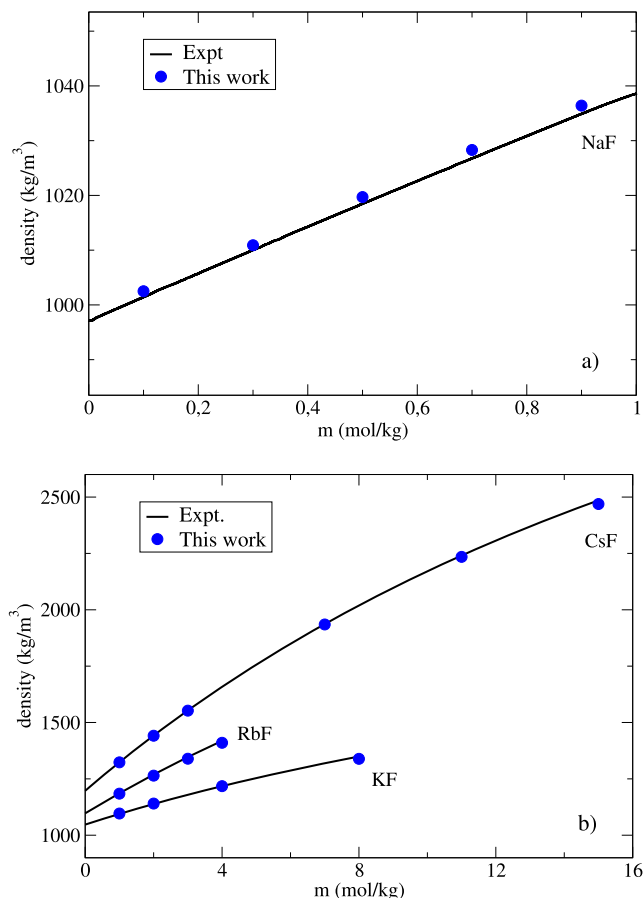


FIG. 3. Density as a function of molality at $T = 298.15$ K and 1 bar. Blue circles: this work. Black solid lines: fit of experimental data taken from Ref. 122 for NaF and KF, Ref. 119 for RbF, and Ref. 123 for CsF. (a) NaF aqueous solutions. (b) KF, RbF, and CsF aqueous solutions. RbF and CsF densities were shifted up 100 and 200 density units, respectively, for a clear visualization.

similar to the one found for the salts included in the original Madrid-2019 force field.⁴⁶ In Fig. 4, we also present the viscosity of the JC-SPC/E model (which uses integer charges), as determined in this work. It is clear that in this case, the viscosity is overestimated at 5 m by a factor of two. Thus, for KF, it seems that the use of scaled charges improves the description of the viscosity. To analyze if the overestimate of the viscosity of KF by the JC-SPC/E is an exception, we have also computed the viscosity of JC-SPC/E for NaCl, which is arguably the most important salt. Somewhat surprisingly, its value at room temperature and pressure and at high concentrations has not been reported before (to the best of our knowledge). The value of the viscosity of NaCl both from the original Madrid-2019 and from the JC-SPC/E model is presented in Fig. 5(a). Again, it is clear that the JC-SPC/E model overestimates the experimental value of the viscosity of NaCl solutions at high concentrations. This is not a problem of the water model as in our previous work, we also showed that the JC model of NaCl overestimates the viscosity even when used with the TIP4P/2005 model of water.⁴⁶ Thus, at least for NaCl and KF, it is

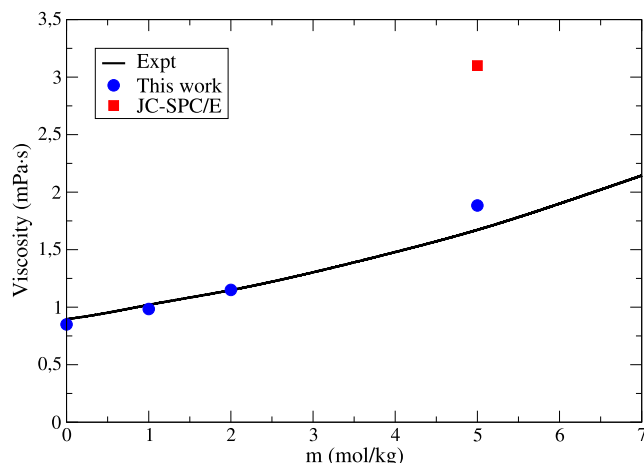


FIG. 4. Shear viscosity curves as a function of concentration for aqueous KF solutions at 298.15 K and 1 bar. The blue circles represent the results from this work. The red squares represent the results for JC-SPC/E model, and the black continuous line represents the fit of experimental data taken from Ref. 124.

clear that the JC-SPC/E model overestimates the value of the viscosity. This overestimation is even greater if we evaluate the ratio of the model viscosity at different concentrations to the model viscosity in pure water, as we can see in Fig. 5(b). This is in line with the results presented by Yue and Panagiotopoulos.⁴⁹ At low concentrations, it was shown that the viscosity of the JC-SPC/E increases faster than that found in experiments and that scaled and polarizable models of NaCl exhibited better (although not perfect) agreement with the experiment.

To complete the study of the fluoride salts with the Madrid-2019-Extended force field, we have analyzed some structural properties. We have calculated the cation–anion, cation–water, and anion–water radial distribution functions close to the experimental solubility limit of each salt.

In Table VI, we have collected all the results obtained for these structural properties and we have compared them with experimental x-ray and neutron diffraction data collected in the work of Marcus.¹²¹ As with the anion–water distances $d_{F^-O_w}$, we see that the value found in this work (around 2.75 Å) is within the experimental reported values of 2.54–2.87 Å. With respect to the cation–water distance, the values found in simulations are, in general, slightly lower (except for K^+) than the lower bound reported in experiments. Similar behavior was found in Madrid-2019 for the Li^+ cation. We do not have an explanation for this. In any case, it seems that the prediction of the distance if wrong does not result in bad predictions for the densities. It can be seen that $d_{cation-O_w}$ increases with the size of the cation. The difference between $d_{K^+-O_w}$ and $d_{Rb^+-O_w}$ distances is small, but as expected, $d_{Rb^+-O_w}$ is larger. With respect to the hydration number, one can see that the F^- anion can be hydrated by about 5.7 molecules of water (see the results for NaF, which is a system without CIPs). For the other salts, it holds that the hydration number of the F^- anion plus the number of CIPs is around 6. Thus, for each molecule of water removed from the hydration shell, a cation occupies its place, indicating that the size of both water and K^+ , Rb^+ , and Cs^+ cations although not identical are not so different. We have

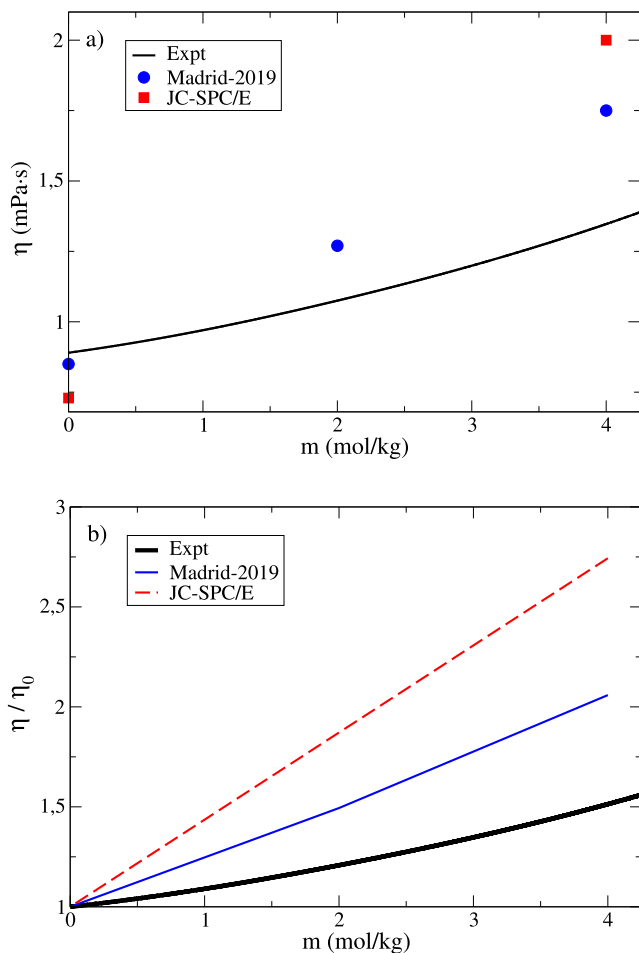


FIG. 5. Viscosity as a function of concentration for NaCl solutions at 298.15 K and 1 bar. (a) Shear viscosity results. The blue circles represent the results from this work with the original Madrid-2019 force field. The red squares represent the results for the JC-SPC/E model, and the black continuous line represents the fit of experimental data taken from Refs. 125 and 126. (b) Ratio of the viscosity at different concentrations to the viscosity in pure water. The blue solid line represents our data for the Madrid-2019 model, the red dashed line represents results for the JC-SPC/E model, and the black solid thick line represents the fit of the experimental data.

to point out that (with the exception of NaF), the rest of fluorides have very high solubility values. Moreover, in the case of RbF, at the solubility limit, the total number of ions is practically equal to the number of water molecules, and in the case of CsF, it is even higher. Thus, we cannot apply the same rules as for other salts, and it is clear that one should allow for a higher number of CIPs. It is also interesting to evaluate what a random mixing model would predict for the number of CIPs. If differences in size between water and the cations are neglected, then one would expect that the number of CIPs would be $6 \cdot (17/55) = 1.85$, $6 \cdot (28/55) = 3.05$, and $6 \cdot (37/55) = 4.03$ for KF, RbF, and CsF, respectively. The number of water molecules that can be located around the F^- anion is 6, and this is multiplied by the ratio of the molality to the number of moles of water in 1 kg. As can

be seen, the random mixing model would predict a number of CIPs higher than found in simulations (1.15, 2.45, and 3.30, respectively, for KF, RbF, and CsF). To be on the safer side, we checked that no spontaneous precipitation occurred at the experimental value of the solubility limit after 50 ns using a large system with 4440 molecules of water.

We shall now present results for the bromide salts.

C. Bromide salts

In Fig. 6(a), we show the results for densities of LiBr, NaBr, and KBr. The solubilities of NaBr and KBr are moderate. The densities obtained for these salts are in excellent agreement with all the experimental data over all the molality range. In the case of LiBr, the simulation results slightly overestimate the experimental ones at intermediate molalities, even though the simulation results are very accurate. In Fig. 6(b), the results for the densities of RbBr and CsBr salt solutions are presented. As can be seen, the results of Madrid-2019-Extended are in reasonable agreement with the experimental ones. It seems that the series of bromides is challenging. In general, the agreement found is good, but sometimes the density is overestimated (as in LiBr) and sometimes is underestimated (as in RbBr and CsBr).

The number of CIPs has been evaluated for these salts and is presented in Table VII. NaBr at 8 m has a number of CIPs of 0.24 and KBr at 5 m has a number of CIPs of 0.29. Both of them follow the rule proposed by Benavides *et al.*¹⁰¹ with a number of CIPs around or below 0.5. The same is true for RbBr and CsBr with a number of CIPs of 0.58 and 0.37, respectively. Thus, for these salts with the solubility smaller than 10 m, the number of CIPs is either around or below 0.5 at the solubility limit. However, for LiBr, with a solubility of 20 m, the number of CIPs is 1.30.

We have also studied divalent salts for bromides. The original Madrid-2019 force field included parameters to describe the interaction between Mg^{2+} with water and between Ca^{2+} with water. Parameters for the $Mg^{2+}-Mg^{2+}$ and $Ca^{2+}-Ca^{2+}$ were also provided in our previous work. The $Br^- - Br^-$ interaction was obtained in this work from the study of 1:1 electrolytes containing Br^- . Thus, for these salts, we can only modify the $Br^- - Mg^{2+}$ and $Br^- - Ca^{2+}$ interactions. As can be seen in Fig. 7, up to 3 m, the results of the force field reproduce the experimental data. At high concentrations, the results are reasonable for the model but tend to slightly underestimate the experimental results in the case of $CaBr_2$ and slightly overestimate them for $MgBr_2$. The number of contact ion pairs for $MgBr_2$ is 0 and for $CaBr_2$ is 0.04. Both salts have a low number of CIPs and do not precipitate. In this respect, bromides behave like chlorides. Both Mg^{2+} and Ca^{2+} have a strong interaction with water, and the cation-anion contact is rare.

Let us now study the behavior of the viscosities for the bromide salts. In particular, we shall analyze LiBr, NaBr, KBr, and $MgBr_2$. The results are shown in Fig. 8. It is interesting that experimentally, LiBr, NaBr, and KBr have a small impact on the viscosity of water (increasing it slightly in the case of NaBr and LiBr), decreasing it slightly in the case of KBr. The Madrid-2019-Extended force field is able to capture this effect. Although the agreement with the experiment is not quantitative, the trends are described quite well. However, adding $MgBr_2$ significantly increases the viscosity of water. Again, this effect is captured by the force

TABLE VI. Structural properties for fluoride electrolyte solutions at 298.15 K (291.15 K for RbF) and 1 bar: number of contact ion pairs (CIPs), hydration number of cations (HN_c) and anions (HN_a), and position of the first maximum of the cation–water (d_{c-O_w}) and anion–water (d_{a-O_w}) interaction in the radial distribution function. Experimental data taken from the work of Marcus are given in parentheses.¹²¹ Properties were calculated close to the solubility limit of each salt and at low concentrations.

Salt	m (mol/kg)	CIP	HN_c	HN_a	d_{c-O_w} (Å)	d_{a-O_w} (Å)
NaF	0.1	0.00	5.5(4–8)	5.8(6–9)	2.33(2.40–2.50)	2.77(2.54–2.87)
	0.9	0.02	5.5	5.8	2.33	2.77
KF	1	0.04	5.7(6–8)	5.7(6–9)	2.73(2.60–2.80)	2.76(2.54–2.87)
	17	1.15	5.8	4.75	2.73	2.75
RbF	1	0.06	6.4(5–8)	5.7(6–9)	2.76(2.79–2.90)	2.77(2.54–2.87)
	28	2.45	4.8	3.45	2.76	2.74
CsF	1	0.05	6.9(8–9)	5.6(6–9)	2.86(2.95–3.20)	2.76(2.54–2.87)
	37	3.30	4.0	2.85	2.86	2.73

field, but it seems that the model overestimates the magnitude of the effect (and the deviation is already visible at 2 m). This is similar to the behavior found for $MgCl_2$. For these salts, $MgCl_2$ and $MgBr_2$, the scaled charges do a good job in describing the

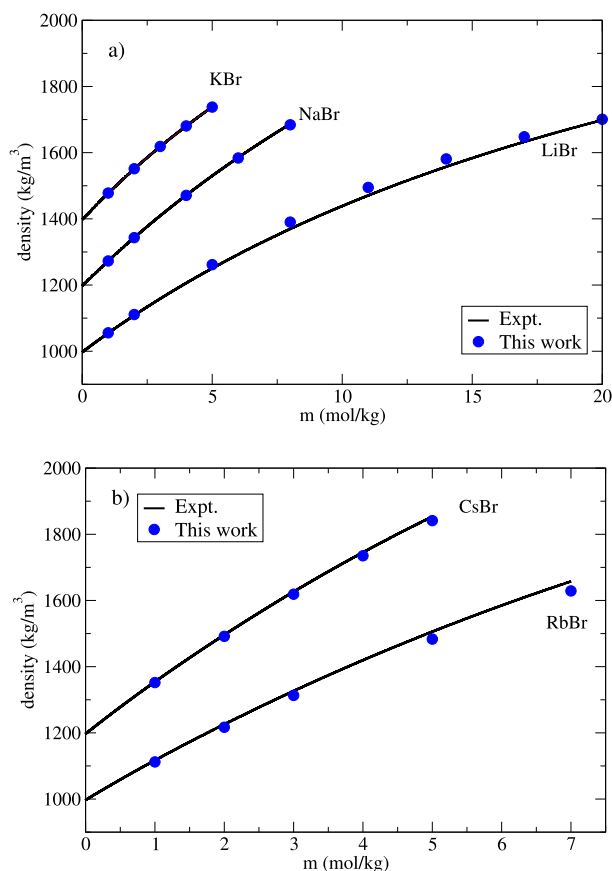


FIG. 6. Density as a function of molality at $T = 298.15$ K and 1 bar for bromide salts of aqueous solutions. (a) LiBr, NaBr, and KBr. (b) RbBr and CsBr. Blue circles: this work. Black solid lines: fit of experimental data taken from Ref. 119 for all salts and Ref. 127 for NaBr and KBr. NaBr and CsBr and KBr densities were shifted up 200 and 400 density units, respectively, for a clear visualization.

experimental values of the viscosities but tend to overestimate their values.

We shall now present (see Table VII) the results for the structural properties. The hydration number of the bromide anion is around 6. Except for LiBr, for the rest of salts, the sum of the hydration number of the anion and the number of CIPs is around 6. That makes sense when taking into account that Na^+ , K^+ , Rb^+ , and Cs^+ have sizes similar to that of water. However, the exception is LiBr. For this salt, at 20 m, one has 7.1 molecules around the Br^- anion, 5.6 molecules of water, and 1.5 molecules of Li^+ . Thus, Li^+ , when in the first coordination of Br^- , provokes a contraction of the molecules of water, hydrating the bromide anion. The bromide–water distance found in this work is within the range of values reported in experiments. For the cations, again, the cation–water distance found in simulation is always slightly below the value reported in experiments. We do not have an explanation for this finding, especially taking into account that the predictions of the densities for bromide salts are quite reasonable.

Finally, in Fig. 9, we show the cation–water radial distribution function as obtained in this work for a 1 m solution of LiBr, NaBr, KBr, RbBr, and CsBr. It can be seen that the distance at which the first peak occurs increases with the size of the cation. The increase is clear for all the cations with one exception. The K^+-O_w and Rb^+-O_w have a similar location of the first peak (i.e., 2.73 vs 2.75 Å, respectively).

D. Iodine salts

We now present the properties for the iodine salts. In particular, we shall consider LiI, NaI, KI, RbI, CsI, MgI_2 , and CaI_2 . Thus, for iodine salts, we present results for a number of cations, including monovalent and divalent cations. We shall start by presenting densities for monovalent ions as obtained from the Madrid-2019-Extended. The results for LiI, NaI, and KI are shown in Fig. 10(a), and the results for RbI and CsI are shown in Fig. 10(b).

LiI, NaI, and KI simulation results are in excellent agreement with the experimental ones for the whole range of molalities. However, at the highest molalities studied for each salt (8 m for KI and 12 m for NaI and LiI), the simulation results slightly overestimate the experimental values. The results for RbI and CsI aqueous solutions are shown in Fig. 10(b). The results for

TABLE VII. Structural properties for bromide electrolyte solutions at 298.15 K and 1 bar: number of contact ion pairs (CIPs), hydration number of cations (HN_c) and anions (HN_a), and position of the first maximum of the cation–water (d_{c-O_w}) and anion–water (d_{a-O_w}) interaction in the radial distribution function. Experimental data taken from the work of Marcus are given in parentheses.¹²¹ Properties were calculated at low concentrations and close to the solubility limit of each salt.

Salt	m (mol/kg)	CIP	HN_c	HN_a	d_{c-O_w} (Å)	d_{a-O_w} (Å)
LiBr	1	0.18	3.8(3.3–5.3)	6.3(4–6)	1.84(1.90–2.25)	3.15(3.01–3.45)
	20	1.5	2.0	5.6	1.84	3.15
NaBr	1	0.02	5.5(4–8)	6.0(4–6)	2.34(2.40–2.50)	3.15(3.01–3.45)
	8	0.24	5.3	6.0	2.33	3.15
KBr	1	0.04	6.7(6–8)	5.9(4–6)	2.73(2.60–2.80)	3.15(3.01–3.45)
	5	0.29	6.4	5.8	2.73	3.15
RbBr	1	0.10	6.3(5–8)	5.8(4–6)	2.76(2.79–2.90)	3.15(3.01–3.45)
	7	0.58	5.8	5.4	2.75	3.15
CsBr	1	0.08	6.7(8–9)	5.9(4–6)	2.85(2.95–3.20)	3.15(3.01–3.45)
	5	0.37	6.2	5.6	2.85	3.15
MgBr ₂	1	0.00	6.0(6–8.1)	5.9(4–6)	1.92(2.00–2.11)	3.15(3.01–3.45)
	5	0.00	6.0	5.9	1.92	3.15
CaBr ₂	1	0.00	7.4(5.5–8.2)	6.1(4–6)	2.38(2.39–2.46)	3.15(3.01–3.45)
	7	0.04	6.9	6.1	2.38	3.15

both salts are in excellent agreement with the experiment for all concentrations.

We shall now turn to salts containing divalent cations. Figure 11 shows the results for the densities of divalent salts of iodide. The results for CaI₂ are in excellent agreement with experimental data over all the molality range. On the other hand, results for MgI₂ overestimate the experimental values at high molalities.

Figure 12 shows the viscosities obtained with the Madrid-2019-Extended force field for NaI and CsI. The agreement is not perfect, but still reasonable. The case of CsI is special because in experiments, the viscosity slightly decreases as the salt concentration increases. The model is not able to capture this decrease in viscosity, but at least

the increase that occurs is very small. The case of NaI is similar to the other salts studied in this work and in the Madrid-2019⁴⁶ force field. The viscosities are well predicted for concentrations of up to 1–2 m and overestimated afterward. The overestimation is not dramatic but seems to be a systematic deviation found in the Madrid-2019-Extended force field. Very little is known about the behavior of the viscosities at high concentrations for most of the force fields of ionic systems. The study of Yue and Panagiotopoulos⁴⁹ and the results for KF and NaCl presented before seem to suggest that integer charges deviate typically more from the experiment than scaled charges. It is also clear that scaled charges improve the description but are not

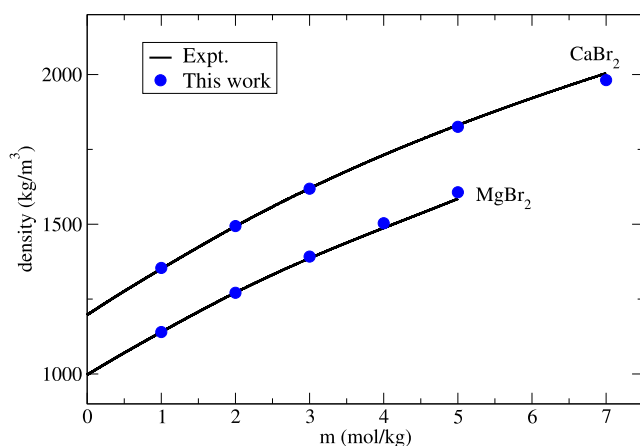


FIG. 7. Density as a function of molality at $T = 298.15$ K and 1 bar for bromide salts of 1:2 aqueous solutions, MgBr₂ and CaBr₂. Blue circles: this work. Black solid lines: fit of experimental data taken from Refs. 119 and 123. CaBr₂ values were shifted up 200 density units for better legibility.

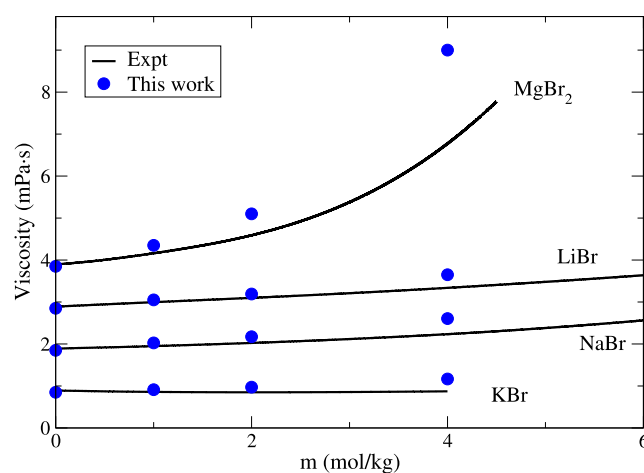


FIG. 8. Shear viscosity curves as a function of concentration for aqueous bromide solutions at 298.15 K and 1 bar. The blue circles represent the results from this work. The continuous lines represent the fit of experimental data taken from Refs. 124, 128, and 129. NaBr, LiBr, and MgBr₂ values were shifted up 1, 2, and 3 viscosity units, respectively, for better legibility.

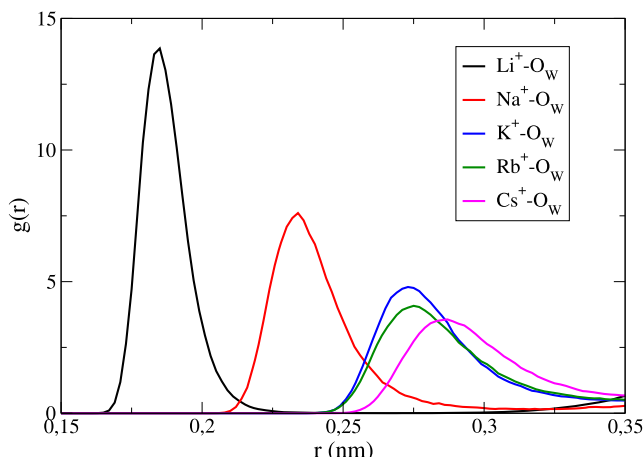


FIG. 9. Cation–water oxygen radial distribution function for bromide solutions at 298.15 K, 1 bar, and 1 m as were obtained with the Madrid-2019-Extended model in following solutions: LiBr, NaBr, KBr, RbBr, and CsBr.

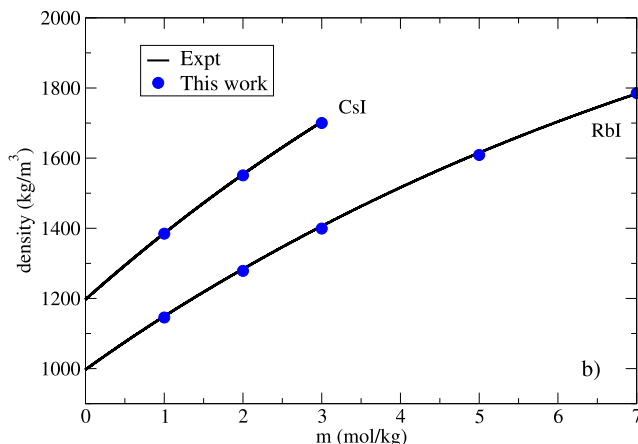
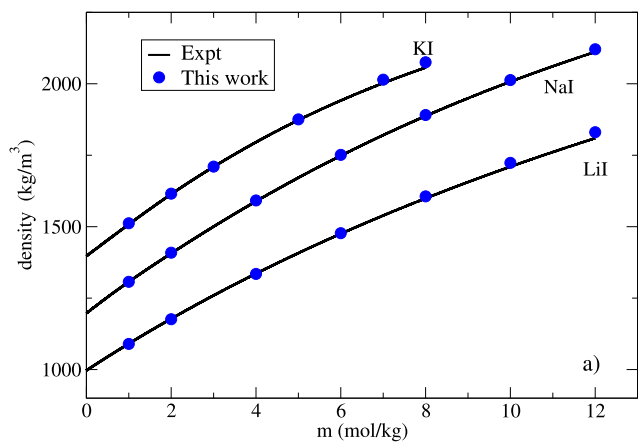


FIG. 10. Density as a function of molality at $T = 298.15$ K and 1 bar for iodide salts of aqueous solutions. (a) LiI, NaI, and KI. (b) RbI and CsI. Blue circles: this work. Black solid lines: fit of experimental data taken from Ref. 119. NaI and CsI densities were shifted up 200 and KI 400 density units for better legibility.

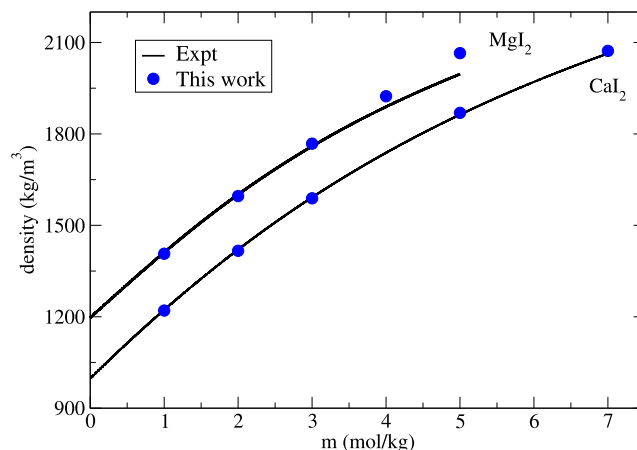


FIG. 11. Density as a function of molality at $T = 298.15$ K and 1 bar for iodide salts of 1:2 aqueous solutions, MgI_2 and CaI_2 . Blue circles: this work. Black solid lines: fit of experimental data taken from Ref. 119. MgI_2 values were shifted up 200 units for better legibility.

able to obtain a full quantitative agreement with the experiment. Note that the deviations are not due to an incorrect prediction of densities. The Madrid-2019-Extended force field yields good prediction of the experimental densities. Therefore, the deviations are due to some missing physics in the model.

Structural properties for iodine salts are presented in Table VIII. The hydration number of iodine is about 6.1 (although this number changes from one salt to another at the high concentrations considered in Table VIII). The number of CIPs is almost zero for Li^+ , Mg^{2+} , and Ca^+ , thus reflecting that these ions are strongly hydrated and CIPs are rare. For the rest of the salts, the number of

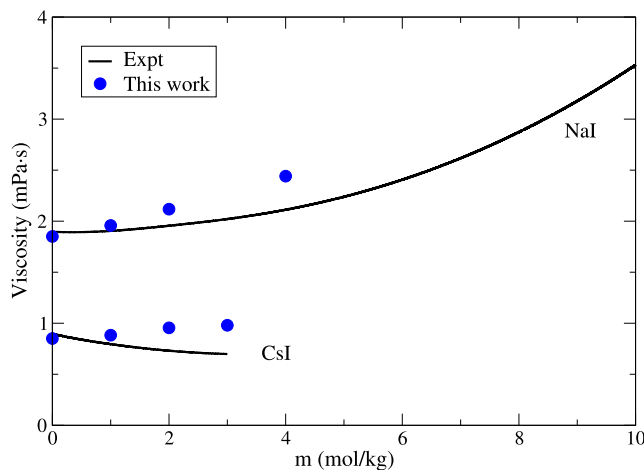


FIG. 12. Shear viscosity curves as a function of concentration for aqueous NaI and CsI solutions at 298.15 K and 1 bar. The blue circles represent the results from this work. The continuous lines represent the fit of experimental data taken from Refs. 126 and 130 for NaI and Ref. 131 for CsI. NaI values were shifted up 1 viscosity unit for better legibility.

TABLE VIII. Structural properties for iodine electrolyte solutions at 298.15 K and 1 bar: number of contact ion pairs (CIPs), hydration number of cations (HN_c) and anions (HN_a), and position of the first maximum of the cation–water ($d_{c-\text{O}_w}$) and anion–water ($d_{a-\text{O}_w}$) interaction in the radial distribution function. Experimental data taken from the work of Marcus are given in parentheses.¹²¹ Properties were calculated at low concentrations and close to the solubility limit of each salt.

Salt	m (mol/kg)	CIP	HN_c	HN_a	$d_{c-\text{O}_w}$ (Å)	$d_{a-\text{O}_w}$ (Å)
LiI	1	0.00	4.0(3.3–5.3)	6.1(4–6)	1.84(1.90–2.25)	3.28(3.01–3.45)
	12	0.01	4.0	6.1	1.84	3.28
NaI	1	0.01	5.5(4–8)	6.1(4–6)	2.33(2.40–2.50)	3.28(3.01–3.45)
	12	1.12	5.3	6.1	2.33	3.28
KI	1	0.03	6.5(6–8)	6.0(4–6)	2.72(2.60–2.80)	3.29(3.01–3.45)
	8	0.30	6.2	6.1	2.72	3.28
RbI	1	0.10	6.3(5–8)	6.0(5.3–7.2)	2.75(2.79–2.90)	3.29(3.08–3.34)
	7	0.60	5.8	5.5	2.75	3.28
CsI	1	0.10	6.6(8–9)	6.0(5.3–7.2)	2.86(2.95–3.20)	3.28(3.08–3.34)
	3	0.35	6.4	5.9	2.86	3.28
MgI_2	1	0.00	6.0(6–8.1)	6.1(4–6)	1.92(2.00–2.11)	3.28(3.01–3.45)
	5	0.00	6.0	6.1	1.92	3.28
CaI_2	1	0.00	7.4(5.5–8.2)	6.0(4–6)	2.38(2.39–2.46)	3.28(3.01–3.45)
	7	0.00	6.9	6.6	2.38	3.28

CIPs is typically below 0.5 at the solubility limit. The main exception to this rule is NaI with a higher number of CIPs.

To finish this section, we shall present results for the anion–oxygen radial distribution function for F^- , Cl^- , Br^- , and I^- . Figure 13 shows the anion–water oxygen radial distribution functions for 1 m sodium salt solutions with the different anions developed in Madrid-2019 and Madrid-2019-Extended force fields. It can be seen that the anion–oxygen distance increases with the size of the anion.

E. Sulfate salts

We shall finish by presenting properties for the sulfate salts. We have included Rb_2SO_4 and Cs_2SO_4 . The results for the densities are

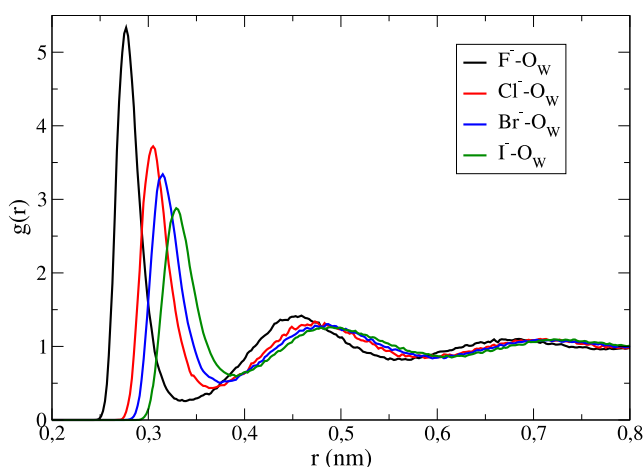


FIG. 13. Anion–water oxygen radial distribution functions for sodium solutions at 298.15 K, 1 bar, and 1 m as were obtained with the Madrid-2019-Extended model in the following solutions: NaF (0.9 m), NaCl, NaBr, and NaI.

in excellent agreement with experimental results, as shown in Fig. 14. Regarding the structural properties (as presented in Table IX), we can observe similar results than those obtained for the sulfate salts studied in the Madrid-2019 force field. The number of contact ion pairs is higher than for other salts. The hydration numbers of the sulfate group are higher than the experimental ones. In our opinion, the results obtained by using simulations are more realistic than the ones from experiments because the size of the sulfate group is too big to have only eight molecules of water around.

F. Density of molten salts

Although the main purpose of using scaled charges is to improve the description of the aqueous solution, we shall now

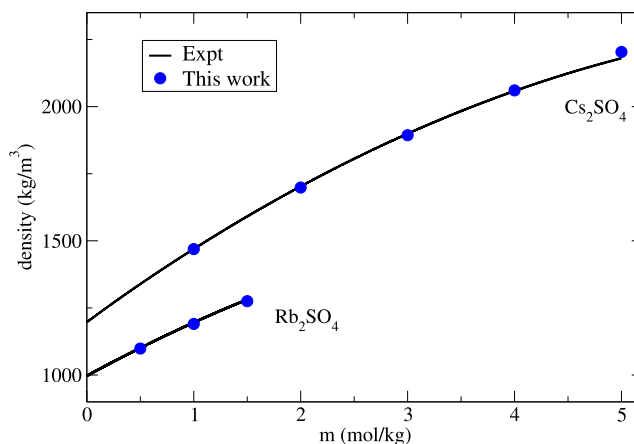


FIG. 14. Density as a function of molality at $T = 298.15$ K and 1 bar for sulfate salts of aqueous solutions, Rb_2SO_4 and Cs_2SO_4 . Blue circles: this work. Black solid lines: fit of experimental data taken from Refs. 119, 132, and 133. Cs_2SO_4 values were shifted up 200 density units for better legibility.

TABLE IX. Structural properties for sulfate electrolyte solutions at 298.15 K and 1 bar: number of contact ion pairs (CIPs), hydration number of cations (HN_c) and anions (HN_a), and position of the first maximum of the cation–water (d_{c-O_w}) and anion–water (d_{a-O_w}) interaction in the radial distribution function. Experimental data taken from the work of Marcus are given in parentheses.¹²¹ Properties were calculated at low concentrations and close to the solubility limit of each salt.

Salt	m (mol/kg)	CIP	HN_c	HN_a	d_{c-O_w} (Å)	d_{s-O_w} (Å)	$d_{O_s-O_w}$ (Å)
Rb ₂ SO ₄	0.5	0.35	6.2(5–8)	12.5(6.4–8.1)	2.75(2.79–2.90)	3.76(3.67–3.89)	3.02(2.84–2.95)
	1.5	0.70	6.0	11.7	2.75	3.77	3.02
Cs ₂ SO ₄	1	0.45	6.5(8–9)	12(6.4–8.1)	2.86(2.95–3.20)	3.78(3.67–3.89)	3.02(2.84–2.95)
	5	1.25	5.8	10.2	2.85	3.76	3.02

present results obtained for the molten salts (at room pressure and at the experimental melting temperature).

In Table X, we have collected the results for the density of the molten salts. As we pointed out in the Madrid-2019 force field, the use of scaled charges improves the description of the aqueous electrolyte solutions but at the cost of correctly describing the properties of the solid and of the melt. In Table X, we can see that the results obtained for the densities of the melt with scaled charges are about 20% or even 25% below the experimental molten densities. When we use a unit charge (with the same parameters as for 0.85 charge), the results are similar to the experimental ones. It is interesting to mention that we have adjusted the cation–cation and anion–anion

TABLE X. Densities of the molten salts (at 1 bar and the experimental melting temperature¹⁰⁶). Values of this work are given under columns labeled q_{sc} and q , which are obtained using scaled charges ($\pm 0.85 Ze$) and integer charges ($\pm 1.0 Ze$) for the ions, respectively. For LiF, the simulation results were obtained at 200 K above the experimental melting temperature. For LiBr, the simulation results were obtained at 3000 bar. For MgBr₂ and MgI₂ chains were observed in the melt reducing the diffusion of ions in the melt.

Salt	Melt density (kg/m ³)		
	Expt.	q_{sc}	q
LiF	1810	1231	1570
LiBr	2528	2220	2445
LiI	3109	2600	3087
NaF	1948	1524	1949
NaBr	2342	1954	2429
NaI	2742	2166	2685
KF	1910	1327	1708
KBr	2127	1634	2090
KI	2448	1825	2325
RbF	2870	2260	2869
RbCl	2248	1547	1986
RbBr	2715	2150	2715
RbI	2904	2279	2876
CsF	3649	2864	3653
CsCl	2790	1989	2568
CsBr	3133	2357	3036
CsI	3197	2479	3191
MgBr ₂	2620	2305	2555
MgI ₂	3050	2693	3004
CaBr ₂	3111	2485	3017
CaI ₂	3443	2766	3335

interactions using the results for the densities of the melt. These interactions have almost no effect on the density of aqueous solution at low concentrations where by far the most important interactions are cation–oxygen and anion–oxygen. However, the parameters of the cation–anion interactions were determined having two properties in mind, namely, the density of the melt and a reasonable number of CIPs at the experimental value of the solubility limit. It should be mentioned that in simulations, we found problems for LiF and LiBr in getting a stable melt at the experimental conditions. In the case of LiF, we found spontaneous crystallization of the molten salt, and for LiBr, we found spontaneous cavitation (due to the formation of chains of ions). For these two salts, our reported simulations were obtained at 200 K above the experimental melting temperature for LiF and 3000 bar at the experimental melting temperature for LiBr (at 1 bar, a 7%–8% lower density is expected, taking into account the experimental behavior of other molten salts).¹³⁴

C. Self-diffusion coefficient of ions at infinite dilution

Let us finish by presenting results for the diffusion coefficient of the ions at infinite dilution. We have performed molecular dynamics simulations of systems with 5550 water molecules and 1 ion in order to study the self-diffusion coefficient of the ion at infinite dilution. The fact that we are using only one ion (we have denoted that as single ion) implies that the system is not electroneutral (although technically the use of Ewald sums implies that one has a neutralizing diffuse background of opposite charge). This is a standard practice done to compute diffusion coefficients at infinite dilution. However, to check for the possible existence of artifacts, we also simulated an electroneutral system having 5550 water molecules, 1 Na⁺ and 1 Cl[−] corresponding to a molality of 0.01 m, and we obtained quite similar results to those obtained with single ion simulations. Thus, we have used the single ion method in the rest of the ions. All the results given in Table XI and presented in Fig. 15 are the result of the average of five independent runs of 40 ns with 5550 water molecules and one ion so that each point obtained is the result of 200 ns of simulation, 2.8 μs in total. For the Madrid-2019 model, we have also included in Table XI the results obtained by Döpke *et al.*,⁴³ obtaining good agreement with ours except for Cl[−] where we obtained a slightly larger value (although still within the combined uncertainty). Note that the results of Döpke *et al.* were obtained using a smaller system having 523 molecules of water.

Figure 15(a) shows that the results for most of the cations (with the exception of Rb⁺) are in excellent agreement with experimental results. It can also be seen that for monovalent cations, the diffusion coefficient increases as the water–cation distance increases. For

TABLE XI. Diffusion coefficients of the Madrid-2019 ions (in cm^2/s) at 1 bar and 298.15 K. We present the results obtained in this work and the results of Döpke *et al.*⁴³ The experimental values are from Ref. 106. The results are obtained from the average of five independent simulations, and we have applied the hydrodynamic corrections of Yeh and Hummer.¹³⁵ The results reported by Dopke *et al.* also include this correction.

Ion	$D_{\text{exp}} \cdot 10^5$	$D_{\text{this work}} \cdot 10^5$		$D_{\text{Dopke}} \cdot 10^5$
		Single ion	Electroneutral	
Na^+	1.334	1.36(07)	1.39(11)	1.28(15)
Cl^-	2.03	1.76(09)	1.75(08)	1.60(08)
K^+	1.957	1.90(11)	...	1.93(06)
Li^+	1.029	1.07(09)	...	1.08(02)
Mg^{2+}	0.706	0.82(07)	...	0.87(13)
Ca^{2+}	0.792	0.84(04)	...	0.89(08)
SO_4^{2-}	1.065	1.27(05)
F^-	1.475	1.36(4)
Br^-	2.080	1.68(5)
I^-	2.045	1.71(6)
Rb^+	2.072	1.88(5)
Cs^+	2.056	1.99(6)

divalent cations, on the other hand, there is no major change in the diffusion coefficient with increasing water–cation distance. In the case of the anions (in particular for halogens), the results obtained are below the experimental ones with the exception of the sulfate in which the opposite is true, as we can see in Fig. 15(b). In this case, the diffusion coefficient increases from the fluorine anion to the chlorine anion and remains constant thereafter. Note that we have applied the hydrodynamic corrections of Yeh and Hummer¹³⁵ using the viscosity of the TIP4P/2005 water model. We have considered that the viscosity of the system is not affected by the presence of one single ion, i.e., at infinite dilution.

H. Diffusion coefficient of water for several salts: Stokes–Einstein relation for aqueous electrolytes

In this work, we have also considered it relevant to analyze the water diffusion coefficients for various aqueous solutions of electrolytes at different concentrations. The salts chosen have been some of those for which we have calculated the viscosity. This is due to the fact that when applying the Yeh and Hummer corrections,¹³⁵ the viscosity used was that of the model. As can be seen in Fig. 16(a), the force field, in the case of KF, is able to reproduce the experimental results accurately (it was the salt that best reproduced the viscosities). Nevertheless, in the case of CsI, we have the same problem that other authors pointed out.⁴⁸ The diffusion coefficient of water in CsI aqueous solutions increases with the concentration. This behavior is anomalous, and capturing the experimental trend is not possible even after using scaled charges. For CsI, the model is able to capture at least a very small impact of the salt on the diffusion coefficient of water. It is true that Ding *et al.*⁶⁹ showed that with *ab initio* calculations, it is possible to reproduce this trend. We have also calculated the diffusion coefficients of water in the presence of other three salts in order to evaluate if the product of the viscosity and the diffusion coefficient of water remains constant (i.e., if the

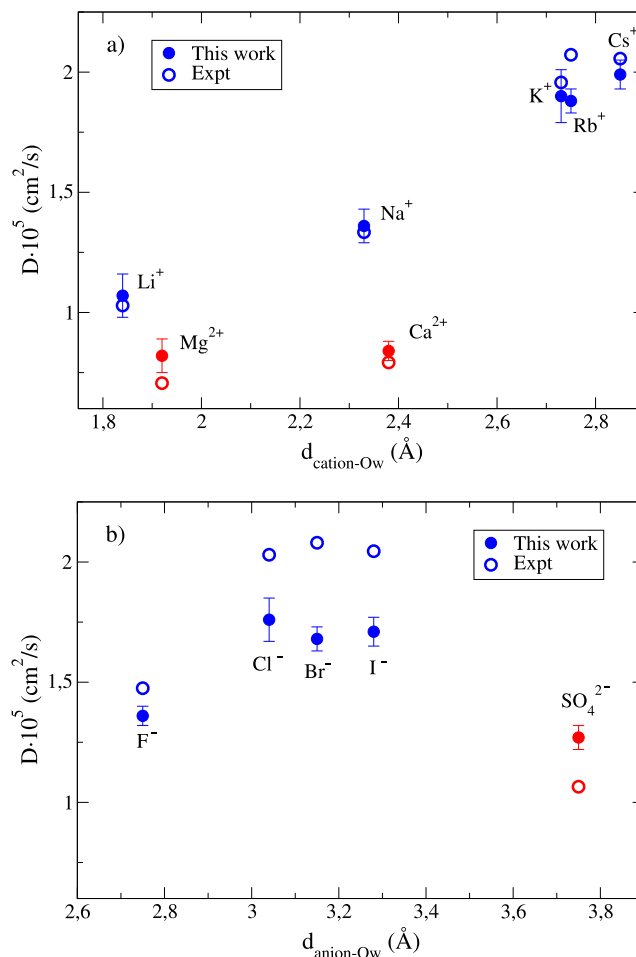


FIG. 15. Diffusion coefficients of the Madrid-2019 ions at 1 bar and 298.15 K (full circles) compared with experimental values¹⁰⁶ (empty circles) in function of the position of the first maximum of the cation–water ($d_{\text{cation-Ow}}$) and anion–water ($d_{\text{anion-Ow}}$) interaction in the radial distribution function. (a) Results for cations. Monovalent cations are shown in blue. Divalent cations are shown in red. (b) Results for anions. Monovalent anions are shown in blue. Sulfate anions are shown in red.

Stokes–Einstein relation⁵⁰ is satisfied). In Fig. 16(b), we have plotted the values of the product of the water diffusion coefficient and viscosity obtained in this work vs salt concentration. It can be seen how all the results follow the same trend and all salts keep the $D \cdot \eta$ product almost constant with a slight increase with the concentration. The experimental results (dashed lines) show the same trend. The agreement between experimental and simulation results for the product $D \cdot \eta$ is excellent. Of course, just because the model reproduces the experimental results of the product $D \cdot \eta$ does not mean that it reproduces the experimental values of viscosity and diffusion coefficients. What happens is that when the force field overestimates the experimental viscosity, to keep constant the product (and reproduce experimental results), the model must underestimate the diffusion coefficients of the water.

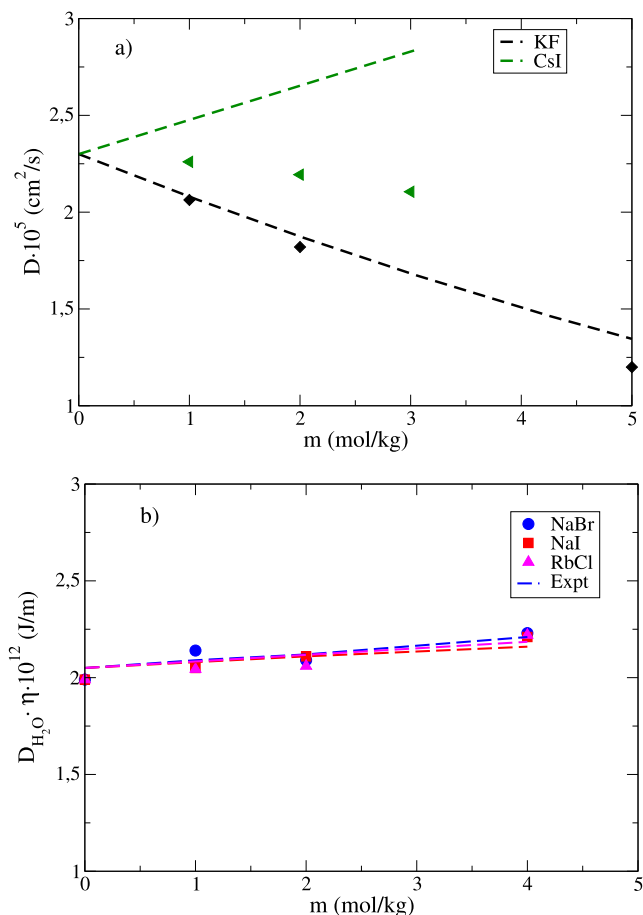


FIG. 16. (a) Diffusion coefficients of water for several salts of the Madrid-2019-Extended at 1 bar and 298.15 K. The green triangles represent the results for CsI, and the black squares represent those for KF. (b) Product of the water diffusion coefficient and viscosity in function of molality for different salts of the Madrid-2019-Extended model: the blue circles represent the results for NaBr, the red squares represent those for NaI, and the pink triangles represent those for RbCl. Experimental results are plotted in dashed lines in the same colors as their respective salts. Experimental diffusion coefficients were obtained from Ref. 136.

V. CONCLUDING REMARKS

In this work, we have developed a Madrid-2019-Extended force field for electrolytes in water (as described by the TIP4P/2005 model). This force field extends the Madrid-2019 force field to the cations Rb^+ and Cs^+ and to the anions F^- , Br^- , and I^- . Thus, the Madrid-2019-Extended force field includes the ions considered in the celebrated Joung–Cheatham force field and some additional ions, such as Mg^{2+} , Ca^{2+} and SO_4^{2-} . We have presented results for the densities of a number of salts and the viscosities for some selected salts. Hydration numbers, radial distribution functions, and contact ion pairs were also calculated, as well as diffusion coefficients of the ions at infinite dilution. The main conclusions of this work are as follows:

- The use of scaled charges allows us to accurately describe the densities of a large number of salts as was already the case with the Madrid-2019 force field.
- As pointed out in the Madrid-2019 force field, the use of scaled charges improves the description of aqueous solutions, but the cost is the description of solid phases: densities for molten salts are underestimated by about 20%.
- Following the philosophy of the Madrid-2019 force field, the charge of 0.85 Z_e quite well describes the viscosities for concentrations of up to 2 m. However, at higher molalities, there are large deviations, especially for divalent salts.
- Self-diffusion coefficients at infinite dilution are accurately described for most of the cations but not for the anions, whose results are slightly worse.
- No spontaneous precipitation was found when performing simulations at the experimental value of the solubility limit.
- The number of CIPs was, in general, below 0.5 for salts with the solubility smaller than 10 m. For salts with huge solubility, this rule cannot be applied. For these salts, the number of CIPs was smaller by about a factor of between 0.6 and 0.8 of that found from the random mixing rule, thus illustrating that water is a good solvent for the ions.

To summarize, the combination of a good model of water and scaled charges yields a reasonable description of electrolyte solutions, improving unit charge force field results. The Madrid-2019-Extended force field should be regarded as a computationally cost-effective way of introducing some degree of polarization. The model provides reasonable results, but for certain properties, the agreement with the experiment is not quantitative, thus showing the limits of this approach. In the particular case of transport properties, it is clear that there is room for improvement. One could argue that polarizable models should improve the description. Time is needed to provide evidence of that. In addition, the impact of nuclear quantum effects on transport properties of electrolytes has not been considered in detail in the literature. For the time being, we hope that the Madrid-2019-Extended, with care, could be useful to provide some predictions regarding interesting physical problems. In the future, it will be useful to study the performance of the Madrid-2019 force field in a number of problems, such as solubilities, freezing point depression, nucleation of ice in salty solutions, and electrical conductivity. A face to face comparison with force fields that use integer charges will bring more evidence of the benefits and drawbacks of using scaled charges.

SUPPLEMENTARY MATERIAL

See the [supplementary material](#) for the numerical results for densities and viscosities obtained in this work for several salt solutions and the complete set of parameters for the force field Madrid-2019 and its extended version and also the `topol.top` file of GROMACS with the force field Madrid-2019 and its extended version attached with this paper.

ACKNOWLEDGMENTS

This work was funded by the MICINN under Grant Nos. PID2019-105898GB-C21 and PID2019-105898GA-C22 and by the

UCM under Grant No. R-910570. M.M.C. acknowledges the CAM and UPM for financial support of this work through CavItieS Project No. APOYO-JOVENES-01HQ1S-129-B5E4MM from “Accion financiada por la Comunidad de Madrid en el marco del Convenio Plurianual con la Universidad Politecnica de Madrid en la linea de actuacion estimulo a la investigacion de jovenes doctores.” S.B. acknowledges the Ministerio de Educacion y Cultura for a pre-doctoral FPU under Grant No. FPU19/00880. The authors acknowledge the Universidad Politecnica de Madrid (www.upm.es) for providing computing resources on Magerit Supercomputer.

AUTHOR DECLARATIONS

Conflict of Interest

The authors have no conflicts to disclose.

DATA AVAILABILITY

The data that support the findings of this study are available within the article and its [supplementary material](#).

REFERENCES

- 1 P. Debye and E. Hückel, *Phys. Z.* **24**, 185 (1923).
- 2 M. J. L. Sangster and M. Dixon, *Adv. Phys.* **25**, 247 (1976).
- 3 M. E. Adams, I. R. McDonald, and K. Singer, *Proc. R. Soc. London, Ser. A* **357**, 37 (1977).
- 4 K. Heinzinger and P. C. Vogel, *Z. Naturforsch., A* **29**, 1164 (1974).
- 5 P. C. Vogel and K. Heinzinger, *Z. Naturforsch., A* **30**, 789 (1975).
- 6 K. Heinzinger and P. C. Vogel, *Z. Naturforsch., A* **31**, 463 (1976).
- 7 W. L. Jorgensen, J. Chandrasekhar, J. D. Madura, R. W. Impey, and M. L. Klein, *J. Chem. Phys.* **79**, 926 (1983).
- 8 H. J. C. Berendsen, J. R. Grigera, and T. P. Straatsma, *J. Phys. Chem.* **91**, 6269 (1987).
- 9 H. W. Horn, W. C. Swope, J. W. Pitera, J. D. Madura, T. J. Dick, G. L. Hura, and T. Head-Gordon, *J. Chem. Phys.* **120**, 9665 (2004).
- 10 M. W. Mahoney and W. L. Jorgensen, *J. Chem. Phys.* **115**, 10758 (2001).
- 11 J. L. F. Abascal and C. Vega, *J. Chem. Phys.* **123**, 234505 (2005).
- 12 C. Vega and J. L. F. Abascal, *Phys. Chem. Chem. Phys.* **13**, 19663 (2011).
- 13 C. Vega, J. L. F. Abascal, M. M. Conde, and J. L. Aragones, *Faraday Discuss.* **141**, 251 (2009).
- 14 W. R. Smith, I. Nezbeda, J. Kolafa, and F. Moučka, *Fluid Phase Equilib.* **466**, 19 (2018).
- 15 J. Chandrasekhar, D. C. Spellmeyer, and W. L. Jorgensen, *J. Am. Chem. Soc.* **106**, 903 (1984).
- 16 T. P. Straatsma and H. J. C. Berendsen, *J. Chem. Phys.* **89**, 5876 (1988).
- 17 J. Aqvist, *J. Phys. Chem.* **94**, 8021 (1990).
- 18 L. X. Dang, *J. Chem. Phys.* **96**, 6970 (1992).
- 19 D. Beglov and B. Roux, *J. Chem. Phys.* **100**, 9050 (1994).
- 20 D. E. Smith and L. X. Dang, *J. Chem. Phys.* **100**, 3757 (1994).
- 21 B. Roux, *Biophys. J.* **71**, 3177 (1996).
- 22 Z. Peng, C. S. Ewig, M.-J. Hwang, M. Waldman, and A. T. Hagler, *J. Phys. Chem. A* **101**, 7243 (1997).
- 23 S. Weerasinghe and P. E. Smith, *J. Chem. Phys.* **119**, 11342 (2003).
- 24 K. P. Jensen and W. L. Jorgensen, *J. Chem. Theory Comput.* **2**, 1499 (2006).
- 25 G. Lamoureux and B. Roux, *J. Phys. Chem. B* **110**, 3308 (2006).
- 26 J. Alejandre and J.-P. Hansen, *Phys. Rev. E* **76**, 061505 (2007).
- 27 P. J. Lenart, A. Jusufi, and A. Z. Panagiotopoulos, *J. Chem. Phys.* **126**, 044509 (2007).
- 28 I. S. Joung and T. E. Cheatham, *J. Phys. Chem. B* **112**, 9020 (2008).
- 29 D. Corradini, M. Rovere, and P. Gallo, *J. Chem. Phys.* **132**, 134508 (2010).
- 30 K. M. Callahan, N. N. Casillas-Ituarte, M. Roeselová, H. C. Allen, and D. J. Tobias, *J. Phys. Chem. A* **114**, 5141 (2010).
- 31 H. Yu, T. W. Whitfield, E. Harder, G. Lamoureux, I. Vorobyov, V. M. Anisimov, A. D. MacKerell, Jr., and B. Roux, *J. Chem. Theory Comput.* **6**, 774 (2010).
- 32 M. M. Reif and P. H. Hünenberger, *J. Chem. Phys.* **134**, 144104 (2011).
- 33 M. B. Gee, N. R. Cox, Y. Jiao, N. Benteñitis, S. Weerasinghe, and P. E. Smith, *J. Chem. Theory Comput.* **7**, 1369 (2011).
- 34 S. Deublein, J. Vrabec, and H. Hasse, *J. Chem. Phys.* **136**, 084501 (2012).
- 35 A. H. Mao and R. V. Pappu, *J. Chem. Phys.* **137**, 064104 (2012).
- 36 S. Mamatkulov, M. Fyta, and R. R. Netz, *J. Chem. Phys.* **138**, 024505 (2013).
- 37 F. Moučka, I. Nezbeda, and W. R. Smith, *J. Chem. Theory Comput.* **9**, 5076 (2013).
- 38 P. T. Kiss and A. Baranyai, *J. Chem. Phys.* **141**, 114501 (2014).
- 39 J. Kolafa, *J. Chem. Phys.* **145**, 204509 (2016).
- 40 R. Elfgen, M. Hülsmann, A. Krämer, T. Köddermann, K. N. Kirschner, and D. Reith, *Eur. Phys. J.: Spec. Top.* **225**, 1391 (2016).
- 41 I. Pethes, *J. Mol. Liq.* **242**, 845 (2017).
- 42 T. Yagasaki, M. Matsumoto, and H. Tanaka, *J. Chem. Theory Comput.* **16**, 2460 (2020).
- 43 M. F. Döpke, O. A. Moulto, and R. Hartkamp, *J. Chem. Phys.* **152**, 024501 (2020).
- 44 A. L. Benavides, J. L. Aragones, and C. Vega, *J. Chem. Phys.* **144**, 124504 (2016).
- 45 A. L. Benavides, M. A. Portillo, V. C. Chamorro, J. R. Espinosa, J. L. F. Abascal, and C. Vega, *J. Chem. Phys.* **147**, 104501 (2017).
- 46 I. M. Zeron, J. L. F. Abascal, and C. Vega, *J. Chem. Phys.* **151**, 134504 (2019).
- 47 I. M. Zeron, M. A. Gonzalez, E. Errani, C. Vega, and J. L. F. Abascal, *J. Chem. Theory Comput.* **17**, 1715 (2021).
- 48 J. S. Kim, Z. Wu, A. R. Morrow, A. Yethiraj, and A. Yethiraj, *J. Phys. Chem. B* **116**, 12007 (2012).
- 49 S. Yue and A. Z. Panagiotopoulos, *Mol. Phys.* **117**, 3538 (2019).
- 50 K. Dill, S. Bromberg, and D. Stigter, *Molecular Driving Forces: Statistical Thermodynamics in Chemistry and Biology* (Garland Science, 2003), ISBN: 9780815320517.
- 51 A. Z. Panagiotopoulos, *J. Chem. Phys.* **153**, 010903 (2020).
- 52 Z. Mester and A. Z. Panagiotopoulos, *J. Chem. Phys.* **143**, 044505 (2015).
- 53 Z. Mester and A. Z. Panagiotopoulos, *J. Chem. Phys.* **142**, 044507 (2015).
- 54 H. Jiang and A. Z. Panagiotopoulos, *J. Chem. Phys.* **145**, 046101 (2016).
- 55 J. R. Espinosa, J. M. Young, H. Jiang, D. Gupta, C. Vega, E. Sanz, P. G. Debenedetti, and A. Z. Panagiotopoulos, *J. Chem. Phys.* **145**, 154111 (2016).
- 56 H. Jiang, Z. Mester, O. A. Moulto, I. G. Economou, and A. Z. Panagiotopoulos, *J. Chem. Theory Comput.* **11**, 3802 (2015).
- 57 N. F. A. van der Vegt, K. Haldrup, S. Roke, J. Zheng, M. Lund, and H. J. Bakker, *Chem. Rev.* **116**, 7626 (2016).
- 58 C. J. Fennell, A. Bizjak, V. Vlachy, and K. A. Dill, *J. Phys. Chem. B* **113**, 6782 (2009).
- 59 Y. Yao and Y. Kanai, *J. Chem. Theory Comput.* **14**, 884 (2018).
- 60 A. A. Chialvo and J. M. Simonson, *J. Chem. Phys.* **124**, 154509 (2006).
- 61 A. K. Giri and E. Spohr, *J. Mol. Liq.* **228**, 63 (2017).
- 62 F. Moučka, I. Nezbeda, and W. R. Smith, *J. Chem. Phys.* **138**, 154102 (2013).
- 63 F. Moučka, M. Lísal, and W. R. Smith, *J. Phys. Chem. B* **116**, 5468 (2012).
- 64 J. Alejandre, G. A. Chapela, F. Bresme, and J.-P. Hansen, *J. Chem. Phys.* **130**, 174505 (2009).
- 65 P. Auffinger, T. E. Cheatham, and A. C. Vaiana, *J. Chem. Theory Comput.* **3**, 1851 (2007).
- 66 T. Martinek, E. Duboué-Dijon, Š. Timr, P. E. Mason, K. Baxová, H. E. Fischer, B. Schmidt, E. Pluhařová, and P. Jungwirth, *J. Chem. Phys.* **148**, 222813 (2018).
- 67 E. Wernersson and P. Jungwirth, *J. Chem. Theory Comput.* **6**, 3233 (2010).
- 68 E. Pluhařová, P. E. Mason, and P. Jungwirth, *J. Phys. Chem. A* **117**, 11766 (2013).
- 69 Y. Ding, A. A. Hassanali, and M. Parrinello, *Proc. Natl. Acad. Sci. U. S. A.* **111**, 3310 (2014).
- 70 P. T. Kiss and A. Baranyai, *J. Chem. Phys.* **138**, 204507 (2013).

- ⁷¹A. Thum, A. Heuer, K. Shimizu, and J. N. Canongia Lopes, *Phys. Chem. Chem. Phys.* **22**, 525 (2020).
- ⁷²C. M. Tenney, M. Massel, J. M. Mayes, M. Sen, J. F. Brennecke, and E. J. Maginn, *J. Chem. Eng. Data* **59**, 391 (2014).
- ⁷³E. E. Fileti and V. V. Chaban, *Chem. Phys. Lett.* **616–617**, 205 (2014).
- ⁷⁴V. V. Chaban, I. V. Voroshylova, and O. N. Kalugin, *Phys. Chem. Chem. Phys.* **13**, 7910 (2011).
- ⁷⁵C. Schröder, *Phys. Chem. Chem. Phys.* **14**, 3089 (2012).
- ⁷⁶I. V. Leontyev and A. A. Stuchebrukhov, *J. Chem. Phys.* **130**, 085102 (2009).
- ⁷⁷I. V. Leontyev and A. A. Stuchebrukhov, *J. Chem. Theory Comput.* **6**, 3153 (2010).
- ⁷⁸I. V. Leontyev and A. A. Stuchebrukhov, *J. Chem. Theory Comput.* **6**, 1498 (2010).
- ⁷⁹I. V. Leontyev and A. Stuchebrukhov, *Phys. Chem. Chem. Phys.* **13**, 2613 (2011).
- ⁸⁰I. V. Leontyev and A. A. Stuchebrukhov, *J. Chem. Theory Comput.* **8**, 3207 (2012).
- ⁸¹I. V. Leontyev and A. A. Stuchebrukhov, *J. Chem. Phys.* **141**, 014103 (2014).
- ⁸²M. Kohagen, P. E. Mason, and P. Jungwirth, *J. Phys. Chem. B* **118**, 7902 (2014).
- ⁸³M. Kohagen, P. E. Mason, and P. Jungwirth, *J. Phys. Chem. B* **120**, 1454 (2015).
- ⁸⁴E. Duboué-Dijon, P. E. Mason, H. E. Fischer, and P. Jungwirth, *J. Phys. Chem. B* **122**, 3296 (2017).
- ⁸⁵Z. R. Kann and J. L. Skinner, *J. Chem. Phys.* **141**, 104507 (2014).
- ⁸⁶C. Vega, *Mol. Phys.* **113**, 1145 (2015).
- ⁸⁷V. Molinero and E. B. Moore, *J. Phys. Chem. B* **113**, 4008 (2009).
- ⁸⁸R. C. DeMille and V. Molinero, *J. Chem. Phys.* **131**, 034107 (2009).
- ⁸⁹R. Fuentes-Azcatl and M. C. Barbosa, *J. Phys. Chem. B* **120**, 2460 (2016).
- ⁹⁰J. Li and F. Wang, *J. Chem. Phys.* **143**, 194505 (2015).
- ⁹¹E. E. Bruce and N. F. A. van der Vegt, *J. Chem. Phys.* **148**, 222816 (2018).
- ⁹²M. Soniat and S. W. Rick, *J. Chem. Phys.* **137**, 044511 (2012).
- ⁹³A. J. Lee and S. W. Rick, *J. Chem. Phys.* **134**, 184507 (2011).
- ⁹⁴M. Soniat and S. W. Rick, *J. Chem. Phys.* **140**, 184703 (2014).
- ⁹⁵M. Soniat, G. Pool, L. Franklin, and S. W. Rick, *Fluid Phase Equilib.* **407**, 31 (2016).
- ⁹⁶Y. Yao, M. L. Berkowitz, and Y. Kanai, *J. Chem. Phys.* **143**, 241101 (2015).
- ⁹⁷E. Duboué-Dijon, M. Javanainen, P. Delcroix, P. Jungwirth, and H. Martinez-Seara, *J. Chem. Phys.* **153**, 050901 (2020).
- ⁹⁸B. J. Kirby and P. Jungwirth, *J. Phys. Chem. Lett.* **10**, 7531 (2019).
- ⁹⁹S. Blazquez, I. M. Zeron, M. M. Conde, J. L. F. Abascal, and C. Vega, *Fluid Phase Equilib.* **513**, 112548 (2020).
- ¹⁰⁰D. Kussainova, A. Mondal, J. M. Young, S. Yue, and A. Z. Panagiotopoulos, *J. Chem. Phys.* **153**, 024501 (2020).
- ¹⁰¹A. L. Benavides, M. A. Portillo, J. L. F. Abascal, and C. Vega, *Mol. Phys.* **115**, 1301 (2017).
- ¹⁰²L. A. Patel and J. T. Kindt, *J. Comput. Chem.* **40**, 135 (2019).
- ¹⁰³H. Jiang, P. G. Debenedetti, and A. Z. Panagiotopoulos, *J. Chem. Phys.* **150**, 124502 (2019).
- ¹⁰⁴A. Nikitin and G. Del Frate, *J. Comput. Chem.* **40**, 2464 (2019).
- ¹⁰⁵M. Vazdar, E. Pluhařová, P. E. Mason, R. Vácha, and P. Jungwirth, *J. Phys. Chem. Lett.* **3**, 2087 (2012).
- ¹⁰⁶W. M. Haynes, *CRC Handbook of Chemistry and Physics* (CRC Press, 2011).
- ¹⁰⁷D. van der Spoel, E. Lindahl, B. Hess, G. Groenhof, A. E. Mark, and H. J. C. Berendsen, *J. Comput. Chem.* **26**, 1701 (2005).
- ¹⁰⁸B. Hess, C. Kutzner, D. van der Spoel, and E. Lindahl, *J. Chem. Theory Comput.* **4**, 435 (2008).
- ¹⁰⁹D. Beeman, *J. Comput. Phys.* **20**, 130 (1976).
- ¹¹⁰S. Nosé, *Mol. Phys.* **52**, 255 (1984).
- ¹¹¹W. G. Hoover, *Phys. Rev. A* **31**, 1695 (1985).
- ¹¹²M. Parrinello and A. Rahman, *J. Appl. Phys.* **52**, 7182 (1981).
- ¹¹³U. Essmann, L. Perera, M. L. Berkowitz, T. Darden, H. Lee, and L. G. Pedersen, *J. Chem. Phys.* **103**, 8577 (1995).
- ¹¹⁴B. Hess, H. Bekker, H. J. C. Berendsen, and J. G. E. M. Fraaije, *J. Comput. Chem.* **18**, 1463 (1997).
- ¹¹⁵B. Hess, *J. Chem. Theory Comput.* **4**, 116 (2008).
- ¹¹⁶M. A. González and J. L. F. Abascal, *J. Chem. Phys.* **132**, 096101 (2010).
- ¹¹⁷G.-J. Guo and Y.-G. Zhang, *Mol. Phys.* **99**, 283 (2001).
- ¹¹⁸D. Alfè and M. J. Gillan, *Phys. Rev. Lett.* **81**, 5161 (1998).
- ¹¹⁹E. W. Washburn, C. J. West, and National Research Council (U.S.), *International Critical Tables of Numerical Data, Physics, Chemistry and Technology* (McGraw-Hill, New York, 1928).
- ¹²⁰A. G. Ostroff, B. S. Snowden, Jr., and D. E. Woessner, *J. Phys. Chem.* **73**, 2784 (1969).
- ¹²¹Y. Marcus, *Chem. Rev.* **88**, 1475 (1988).
- ¹²²T. G. Pedersen, C. Dethlefsen, and A. Hvidt, *Carlsberg Res. Commun.* **49**, 445 (1984).
- ¹²³P. Novotny and O. Sohnel, *J. Chem. Eng. Data* **33**, 49 (1988).
- ¹²⁴D. E. Goldsack and R. C. Franchetto, *Can. J. Chem.* **56**, 1442 (1978).
- ¹²⁵M. Laliberté, *J. Chem. Eng. Data* **52**, 321 (2007).
- ¹²⁶M. Laliberté, *J. Chem. Eng. Data* **52**, 1507 (2007).
- ¹²⁷T. Isono, *J. Chem. Eng. Data* **29**, 45 (1984).
- ¹²⁸I. D. Zaitsev and G. Aseev, *Properties of Aqueous Solutions of Electrolytes* (CRC Press, Boca Raton, 1992), ISBN: 0849393140.
- ¹²⁹A. Lo Surdo and H. E. Wirth, *J. Phys. Chem.* **83**, 879 (1979).
- ¹³⁰I. M. Abdulagatov, A. B. Zeinalova, and N. D. Azizov, *J. Chem. Eng. Data* **51**, 1645 (2006).
- ¹³¹G. Jones and H. J. Fornwalt, *J. Am. Chem. Soc.* **58**, 619 (1936).
- ¹³²D. B. Ludlum and R. C. Warner, *J. Biol. Chem.* **240**, 2961 (1965).
- ¹³³K. Sun, Z. Bi, Y. Meng, Y. Guo, L. Meng, and T. Deng, *J. Chem. Thermodyn.* **161**, 106519 (2021).
- ¹³⁴G. Goldmann and K. Tödheide, *Z. Naturforsch., A* **31**, 769 (1976).
- ¹³⁵I.-C. Yeh and G. Hummer, *J. Phys. Chem. B* **108**, 15873 (2004).
- ¹³⁶K. J. Müller and H. G. Hertz, *J. Phys. Chem.* **100**, 1256 (1996).